THESIS

OPERATIONAL CONDITIONS FOR AN INTERNAL COMBUSTION ENGINE IN A SOFC-ICE HYBRID POWER GENERATION SYSTEM

Submitted by

Victor A. Reyes-Flores

Department of Mechanical Engineering

In partial fulfilment of the requirements

For the Degree of Master of Science

Colorado State University

Fort Collins, Colorado

Spring 2025

Master's Committee:

Advisor: Todd Bandhauer

Daniel B. Olsen
Jeremy Daily

ABSTRACT

OPERATIONAL CONDITIONS FOR AN INTERNAL COMBUSTION ENGINE IN A SOFC-ICE HYBRID POWER GENERATION SYSTEM

Hybrid power generation systems utilizing pressurized solid oxide fuel cells (SOFC) have gained considerable attention recently as an effective solution to the increasing demand for cleaner electricity sources. Among the various hybridization options, gas turbines (GT) and internal combustion engines (ICE) running on off SOFC tail gas have been prominent. Although spark ignition (SI) tail gas engines have received less focus, they show significant potential for stationary power generation, particularly due to their ability to control combustion. This research experimentally characterized an SI engine fueled by simulated SOFC anode gas across a range of variations with fuel cell loads. The study aimed to optimize the engine operating conditions for each fuel blend and establish operational conditions that would sustain maximum performance. The results showed efficiencies as high as 31.4% at 1600 rpm, with a 17:1 compression ratio, equivalence ratio (φ) = 0.75, and a boost pressure of 165 kPa with low NOx emissions. The study also emphasizes the benefits of optimizing boost supply to minimize parasitic loads and improve brake thermal efficiency (BTE). Additionally, installing a catalytic oxidizer would enable the system to comply with new engine emission regulations. A proposed control scheme for automation includes regulating engine power by controlling the boost of the supercharger at a fixed throttle position.

ACKNOWLEDGEMENTS

It has truly been a privilege to pursue a graduate program. Often, we take for granted the things we have, never stopping to reflect on those who helped us get here. The first people I must acknowledge are my mom, Brenda Flores-Ortiz, my dad, Victor Manuel Reyes-Figueroa, and my grandma, Maria Cristina Ortiz-Matos. Without their unwavering support throughout my education, I wouldn't be where I am today. From buying me my first car, covering my expenses, preparing meals for me every weekend until I graduated, to being there for me through it all—these are gifts that few are fortunate enough to experience. The simple fact of having a loving and healthy family is something to be grateful for, but you all went far beyond that for me, and I will never forget it.

I also want to thank my sister, Carla Patricia Reyes-Flores. I'll never forget the time when I started university and felt completely overwhelmed. I went to your room, vented for what felt like hours, and just having you listen to me was enough to help me keep going. The little moments of distraction, like popping into your room while you were studying, helped me more than you know. Thank you for always being there for me when I needed it most.

To Karina Alejandra Concepcion-Nazario: you have been my rock throughout the past few years. Moving to the U.S. was one of the most challenging experiences I've faced, but you made it so much easier. If I thank my family for supporting me during my bachelor's degree, I must thank you for getting me through my master's. Having someone to share the experience of culture shock with in Fort Collins, someone to laugh with during tough times, and someone who I knew would always have my back—this has meant everything to me. I can't fully express how much I appreciate all that you've done for me.

I also want to thank the REACH CoLab for giving me the opportunity to start my master's degree and for the support in helping me complete it. A special thanks goes to Shane Garland, who served as my guide throughout the entire journey. His mentorship was a key factor in my success. Since the Research Experience for Undergraduates in 2021, he's taught me what it means to be a good engineer. The seemingly small tasks that I once overlooked turned out to be invaluable in helping me develop skills I never anticipated gaining. Working alongside him also gave me the chance to approach problems from different perspectives. I faced many challenges in my work and often felt like giving up, but through it all, Shane was always there, willing to help troubleshoot and find solutions together. He is truly an indispensable part of the team. I also want to thank Maddy Siegel, Taylor Stoll, Lars Mitchel, Frederick Schmid, and Ben Platt for their support. Not only did they help me with my classes and research, but they also provided much-needed emotional support. From mountain biking to playing Magic: The Gathering, those moments of connection helped more than I ever could have imagined.

I'd also like to recognize a few other people: Chris Lute, for always resolving my LabView issues; Don Grove, for helping me track down the nearly impossible-to-find trim valve; and Dr. Olsen and Dr. Windom, for their invaluable support throughout my research.

Lastly, I want to thank my friends back in Puerto Rico. Even though many of you didn't know the struggles I faced at CSU, being able to take a break, forget about my problems, and play games with you all was like a therapy session I didn't know I needed. There are many more people I would like to acknowledge, but if I listed everyone, this acknowledgment would be longer than the thesis itself!

This experience has impacted me both professionally and personally. I've often said that if it weren't for this experience, I would have been the worst engineer. The skills I've developed here

are ones I'll carry with me forever. Personally, it has taught me to focus on what truly matters. My perspective has completely changed compared to two years ago, and I'm deeply grateful for the growth this experience has brought me. It has been a pleasure to be part of the REACH CoLab, and I wish nothing but the best for everyone involved.

TABLE OF CONTENTS

LIST OF TABLES

LIST OF FIGURES

NOMENCLATURE

Symbol	Description	Unit
X_{i}	*mole fraction*	-
MW_{i}	*molar weight of the constituent*	g/mol
MW_{f}	*molar weight of the fuel*	g/mol
Y_{i}	*mass fraction*	-
LHV_{i}	*low heating value of the constituent*	kJ/kg
LHV_{f}	*low heating value of fuel*	kJ/kg
W_{e}	*power output*	kW
η_{g}	*alternator efficiency*	%
m_{f}	*fuel flow*	g/s
τ_{Brake}	*brake torque*	N*m
N	*revolutions per minute*	rpm
BTE	*brake thermal efficiency*	%

CHAPTER 1. INTRODUCTION

1.1 Background

SOFC hybrid power generation systems had been a subject of interest in recent years as a solution to the increasing demand for cleaner sources of electricity. With the current electrification efforts to move away from fossil fuels, the United States Government (U.S.) had set goals for clean electricity by 2035 and net-zero emissions by 2050 [1]. However, as of 2023, the U.S. relied on 12,538 power plants generating approximately 4,178 billion kilowatt-hours a year, of which over 3,400 used fossil fuels as their main power source. These fossil fuel plants produced around 60% of the electricity generation whereas the other 40% was generated by renewable energies and nuclear power, as shown in Figure 1 [2,3].

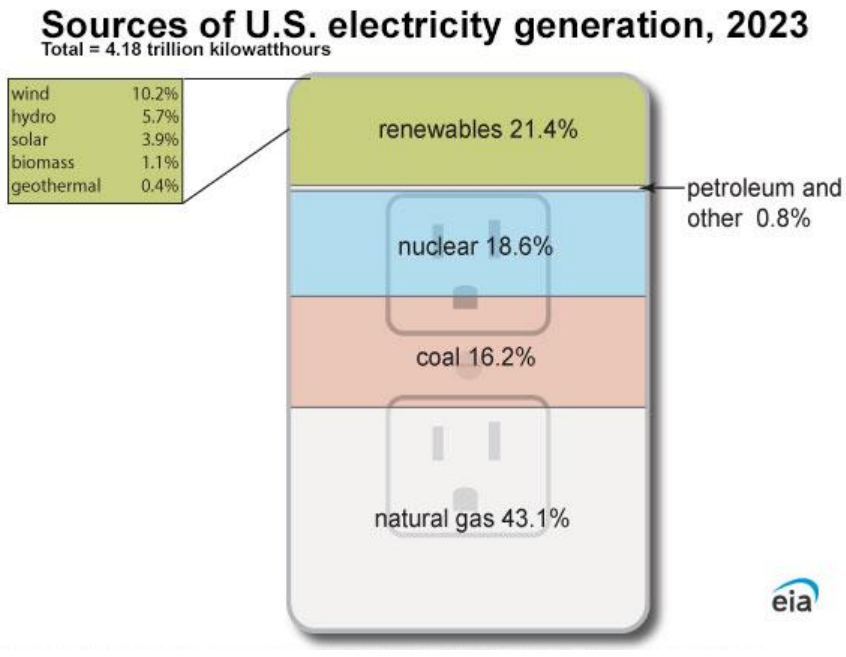

Figure 1. Electricity generation sources in the US in 2023

As a result of the high dependency on fossil fuels, the U.S. has been reducing its emissions to keep up with the electricity demand as they work to find better alternatives for electricity production. The U.S. Environmental Protection Agency (EPA) published a report showing reductions up to 50% in many pollutants from their power plants, such as sulfur dioxide (SO2), nitrogen oxides (NOx), carbon dioxide (CO2), and mercury (Hg), from 2017 to 2023 [4], but to achieve net-zero by 2050, it is crucial to find cleaner ways to produce sustainable electricity and eliminate the use of fossil fuels. SOFC-based systems have the potential to operate at high efficiency and can be scaled to meet the electricity demand depending on the application. Halinen [5] tested and deployed a 10kW SOFC system that operated with natural gas (NG) for over 1500hr at an efficiency of 60%. Other examples, such as L. Barelli [6] have developed models to understand the benefits of a hybrid SOFC-GT system in microgrids. Their results showed a guaranteed mean efficiency of 54.5% with short time response for 95kW of electrical output. Lastly, Colón Rodríguez J. [7] modeled a 100kW SOFC hybrid system coupled with an internal combustion engine (ICE) that was able to achieve efficiencies of 62%. These studies demonstrate the possibilities that these type of systems have for future power generation.

The proposed system is an SOFC- ICE hybrid generator funded under the ARPA-e INTEGRATE program that harnesses the exhausted anode gas in a SI engine to generate supplemental power. Figure 2 shows a diagram of the system. The hybrid system begins by processing the NG entering the system to remove any impurities that could advance the degradation of the SOFC modules. The natural gas enters the recycle loop which is preheated and sent to the SOFC. After the SOFC uses the majority of the available fuel, high temperature anode gas (~ 630° C) is redirected back through the recycle loop to heat up the incoming fuel. A portion of anode gas is directed to an SI engine to combust the remaining fuel. The power produced by the

engine is turned into electricity, which is used to power the auxiliary components needed for SOFC operation, increasing the overall efficiency of the system. The combination of these techniques and other optimization to the auxiliary components (compressors, heat exchangers, etc.) have the possibility of archiving an overall system efficiency > 70% of the lower heating value (LHV) at a cost < 900 $/kW with low emissions [8].

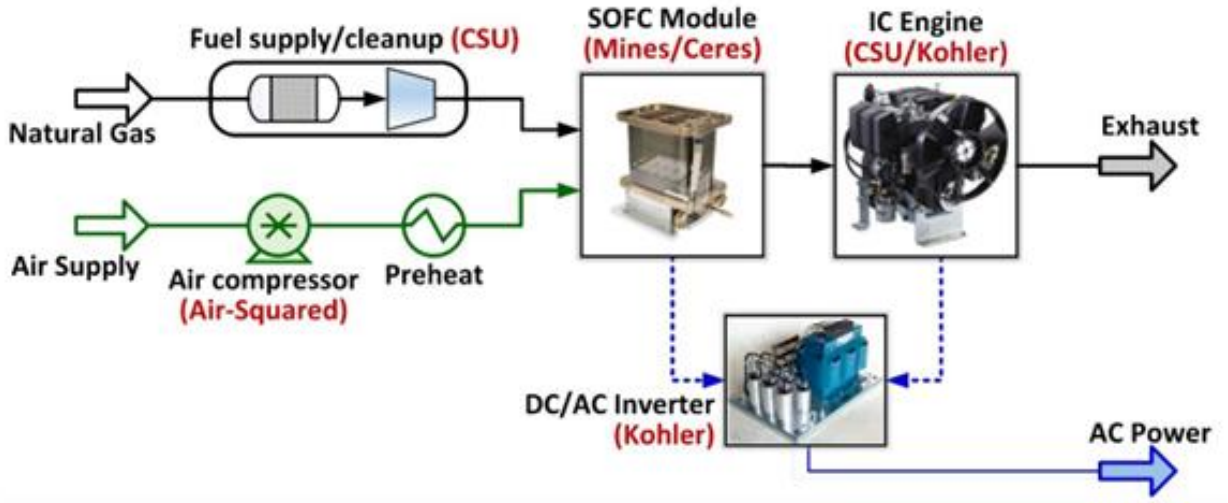

Figure 2. SOFC-ICE facility diagram.

1.2 Research Objectives

The purpose of this research was to experimentally test the SI engine within the hybrid system over a range of expected fuel compositions, optimize the engine for varying anode tail gas blends, and generate a set of operational conditions that could sustain maximum performance during operation. The optimization included finding the best spark timing to achieve maximum power generation, adjusting supercharger boost to reduce power losses, analyzing emissions data for all fuel blends, and performing a speed sweep to choose the optimal RPM. These tests provide a deeper understanding of SIs running with anode fuels, as this technology is the least researched in SOFC hybridization. Additionally, the testing offers insights into a potential engine control

scheme for the current SOFC-ICE hybrid facility. The findings of this research could also be used as the foundation of a future automated control scheme for anode fueled engines. The next sections of the paper will cover the test facility, the methodology used for data analysis, and a discussion of the results from the experimental data.

1.3 Theses Organization

The thesis is structured into several chapters, each addressing different aspects of the research including the motivation behind the study, the test facility, methodology, and an overview of the results and discussions. Chapter two focuses on explaining the operation of the system and the various configurations of SOFC hybrid systems. It includes a literature review of relevant projects that have explored similar generators, comparing them to the proposed study. Chapter three describes the test facility, and the instrumentation used during testing, providing essential information and data to understand the function of each component. Chapter four presents the key equations, technical details, and testing and analytical strategies employed. Chapter five discusses the results of the tests, with a detailed analysis that highlights the most relevant findings from the data acquired. Chapter six draws the study's conclusions and offers recommendations for future work aimed at further optimizing the engine and its controls.

CHAPTER 2. LITERATURE REVIEW

2.1 SOFC for Power Generation

SOFCs electrochemically convert fuel into electricity and can operate on carbon-based fuels through processes such as steam methane reforming and the water gas shift reaction [9]. These processes can be highly efficient which significantly reduces emissions over conventional combustion-based sources. For these reasons, along with other advantages over current technologies—such as fuel flexibility, high efficiency, and scalability—SOFCs could serve as a critical steppingstone toward cleaner electricity generation. Figure 3 showed a report by IDTechEx on how SOFCs could use hydrocarbons as fuel, such as natural gas (NG) and biofuels, but also use zero/low emissions fuels like hydrogen (H2) and ammonia (NH4) [10].

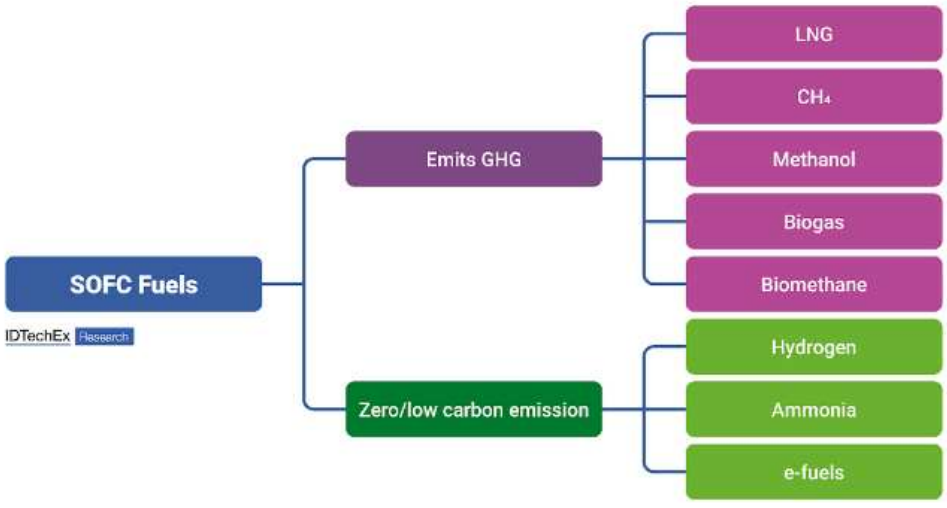

Figure 3. IDTechEx report on possible sources of fuel for SOFC systems.

Additionally, studies had demonstrated SOFCs reaching an electrical efficiency of 50 - 60% depending on the conditions, with possibilities of increasing it even further with other techniques, such as pressurization and hybridization [11–13]. Another advantage that SOFCs have over other technologies is their emissions. A document published by the EPA states that any fuel cell system, including SOFCs, does not require any emissions control devices because these systems already meet future emissions regulations [14]. Table 1 showed data from said document showing fuel cell technologies and their respective emissions.

Table 1. Estimated emissions from different fuel cell technologies. Data provided by IFC Manufacture Data Collection.

Emissions Characteristics	System 1	System 2	System 3	System 4	System 5
Fuel Cell Type	PEMFC	SOFC	MCFC	PAFC	MCFC
Nominal Electricity Capacity (kW)	0.7	1.5	300	400	1,400
NO_x (lb/MWh)	Negligible	Negligible	0.01	0.01	0.01
SO_x (lb/MWh)	Negligible	Negligible	0.0001	Negligible	0.0001
CO (lb/MWh)	Negligible	Negligible	Negligible	0.02	Negligible
VOC (lb/MWh)	Negligible	Negligible	Negligible	0.02	Negligible
CO_2 (lb/MWh)	1,131	734	980	1,049	980
CO_2 with heat recovery (lb/MWh)	415	555	520-680	495	520

On the other hand, SOFCs have the disadvantage of durability. Typical SOFCs are made with ceramic for their supports because of the high temperatures (900 – 1000°C) required for operation. These supports are prone to cracking due to heat cycles or vibrations, making SOFCs not robust enough for prolonged energy generation. With technological advances and pressurization techniques, current SOFC technologies can operate at lower temperatures, and metal supports have become viable [15]. Given this information, SOFCs' higher efficiency, lower emissions and scalability made it a compelling technology to study for power generation [16].

2.2 SOFC Hybrid Systems

Hybridizing SOFCs is one of the most effective ways to increase the systems' overall efficiency. Many configurations exist for hybridization, but the main technologies used for SOFC hybrid power systems are gas turbines (GTs) and internal combustion engines (ICEs). Both technologies have advantages, such as SOFC-GT systems being better for large scale power production, while SOFC-ICE systems are more effective in small scale power generation [17]. In the following subsections, a more detailed explanation of how these systems work will be provided.

2.2.1 SOFC-GT Hybrid Systems

SOFC-GT hybrid systems typically work by first providing fuel to the SOFC for the electrochemical process. After this process concludes, the exhausted anode gas from the SOFC is routed into a combustor to oxidize the remaining constitutes in the blend. The oxidized products are then sent into a turbine to generate supplemental power for the sub-systems, increasing the overall efficiency [9]. Figure 4 shows the architecture of a pressurized SOFC-GT system project being developed by Czero.

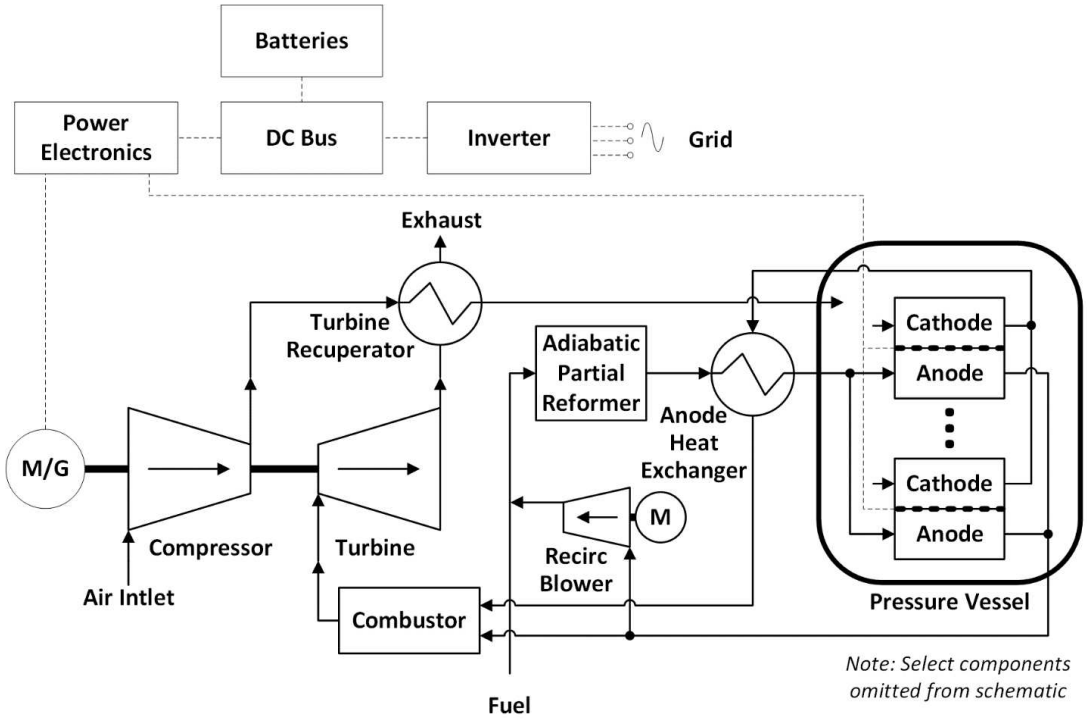

Figure 4. Czero's SOFC-GT system architecture [9].

Additional to the Czero project, other studies have shown great results using this type of system [18–20]. For example, Mitsubishi Heavy Industries published experimental data from a 200-kW class SOFC-GT system showing an overall efficiency of 50% LHV with claims of over 70% LHV efficiency at the MW scale running with NG [21]. Regarding emissions, SOFC-GTs had been found to produce less than 1 ppm of NOx when the GT was positioned downstream of the SOFC [18]. Therefore, it was reasonable to assume that the emissions for the system would be in that same range. Another relevant study was a model developed by The Alaska Center of Energy and Power that tackles the biggest disadvantage of SOFC-GT systems, demand fluctuations. The result of this study shows a maximum overall efficiency of 62.85% at 126.7kW with a turn-down ratio of 5:1, giving the system the capability to maintain this level of performance at 5%± of its design target. [22]. Considering the literature, GTs are a very promising technology to couple with

SOFC, but they come with a set of integration challenges. GTs control schemes are complex, especially when operating conditions change, making the hybridization process more difficult. In a SOFC hybrid power generator, it was possible for demand fluctuations to occur, reducing the overall efficiency of the system if operational conditions deviated too much from the design point. Even though models have been developed to increase the operational range, experimental data is still required to confirm improvements. Also, GTs are much more expensive than ICE, increasing the $/kW. Hence, GTs were not the most desirable technology for this application. [23–26].

2.2.2 SOFC-ICE Hybrid Systems

In contrast, typical SOFC-ICE systems follow a process similar to that described for the GT system, but the exhaust gas from the anode flows into an engine to generate supplemental power. The two primary engine technologies commonly used for hybridization are homogeneous charge compression ignition (HCCI) and spark ignition (SI). HCCI engines are a type of compression ignition (CI) engine that uses a homogenous mix of air and fuel that, when introduced into the cylinder, auto-ignites near the end of the compression stroke, managing low temperature combustion and, subsequently, low emissions, while SIs uses an external power source, such as a spark plug, for ignition. Figure 5 shows the difference in combustion strategies.

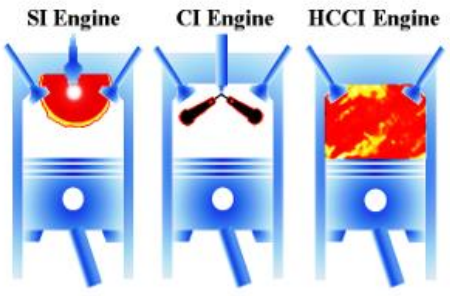

Figure 5. Combustion characteristics of SI, CI and HCCI engines [27].

Understanding the difference between the two technologies is key to comprehending how each system interacts with SOFCs in hybrid applications.

2.2.3 Current Research in SOFC-ICE Hybrid Power Generation

SOFC-HCCI hybrid systems have been the focus of many studies [28–32]. One such study, conducted by Seoul National University, combined the first attempt to acquire experimental data from a single-cylinder HCCI engine running on anode gas with SOFC model data for a 5-kW class system to assess design point performance. Their results showed a system capable of producing power at an efficiency of 59% with less than 1 ppm of NOx and CO emissions [33,34]. This study considered anode gas composition variation and flow rates based SOFC fuel utilization. The engine performance exhibited a gross indicated efficiency of 25 - 30% under stable combustion. Yet, one of the biggest drawbacks of HCCI engines emerged during testing, combustion control. The research indicates that CO emissions and the coefficient of variance in the indicated mean effective pressure were challenging to control, due to the influence of peak in-cylinder temperatures and load, respectively. These results experimentally demonstrate the sensitivity of HCCIs to temperature and pressure, both of which are crucial for auto-ignition [35–37]. Since there is no direct way to control ignition, these two properties need to be at a certain range for the engine to combust the fuel mix, having similar problems as GTs when the conditions diverge from the design point. In a configuration where the engine is downstream of the SOFC, their narrow range of operations could cause issues since both properties are dependent on SOFC fuel utilization.

However, Seoul National University also investigated how SI performance compared to HCCI by replacing and experimentally testing their models with an SI combustion strategy. They demonstrated comparable performance and emissions to HCCI without the added complexity of controls, and they improved their SOFC-ICE model, achieving an overall system efficiency of

63.2%, up from the previously reported 59% [38,39]. Thought the experiment assumed that the gas composition and flow rate of anode gas being exhausted by the SOFC was constant. As mentioned earlier, the load on SOFCs can vary during operation, which directly impacts fuel utilization and, in turn, alters flow rates and gas composition. Another institution that has experimentally tested SIs is Stony Brook University. They tested a cooperative fuel research (CFR) engine with anode gas, achieving a fuel conversion efficiency of 31.3% with low emissions [40]. After these findings, they continue their efforts by testing a SI engine running with one fuel blend representative of anode gas at a constant mass flow to compare the performance at three different water vapor rates. The results showed a maximum brake thermal efficiency (BTE) of 33.9% as part of a 1.1 MW SOFCI-HCCI model system with an estimated electrical efficiency of 70% [41]. The constant composition and fuel flow assumptions were beneficial for this research as their intentions were to study how the water content of the fuel mix would affect the engine's performance, but it does not test realistic conditions of this type of system. All SI experiments also demonstrated low emissions, strongly supporting SIs as one of the most promising combustion strategies for SOFC hybridization. While these results are promising for SIs, there is still a lack of data on the feasibility of using an SI with a dynamic fuel composition.

2.2.4 Gaps in Literature for SOFC-ICE Hybrid Power Generation

After reviewing the literature, all three technologies had their advantages and disadvantages for the purpose of hybridization. Table 2 shows a comparison between what has been studied and the proposed research.

Table 2. Summary of SOFC Hybrid power systems.

Author	Power Target	Engine Type	Composition Variation	Optimize	Control Strategy	Load Variation
Park et al.	14kW	HCCI				
Zhu et al.	150kW	HCCI				
D.F. et al.	100kW	HCCI				
Koo et al.	5kW	HCCI				
Choi et al.	10kW	HCCI	X	X		
Kim et al.	5kW	SI		X		
Ran et al.	-	CFR-SI		X		
Nikiforakis et al.	-	SI	X	X		
Colorado State University						
Padahi et al.	-	CFR-SI				
Balu et al.	4kW	CFR-SI	X	X		
Countie et al.	14kW	SI		X		
Valles Castro et al.	14kW	SI				
This study	8kW	SI	X	X	X	X

Despite being the least studied among the three and still having integration difficulties, SIs showed considerable potential for stationary power generation. One of the biggest gaps found during the literature review process was the lack of control strategies for SI engines running with dilute fuels, dynamic fuel compositions testing and load variability. For such technologies to

mature, it is important to understand what shortcomings are present in the system that would interfere with the engine's operation, such as demand changes. Additionally, analyzing the engine's subsystems, such as the throttle body behavior and sensors, would also help determine what are the best operational conditions for the engine to be at for sustained highest performance, regardless of the fuel composition and load. With the data gathered during this research, a possible control and automation strategy could be developed for engines running with anode gas.

CHAPTER 3. TEST FACILITY

3.1 Facility Overview

A facility diagram that depicting the system components can be seen in Figure 6.

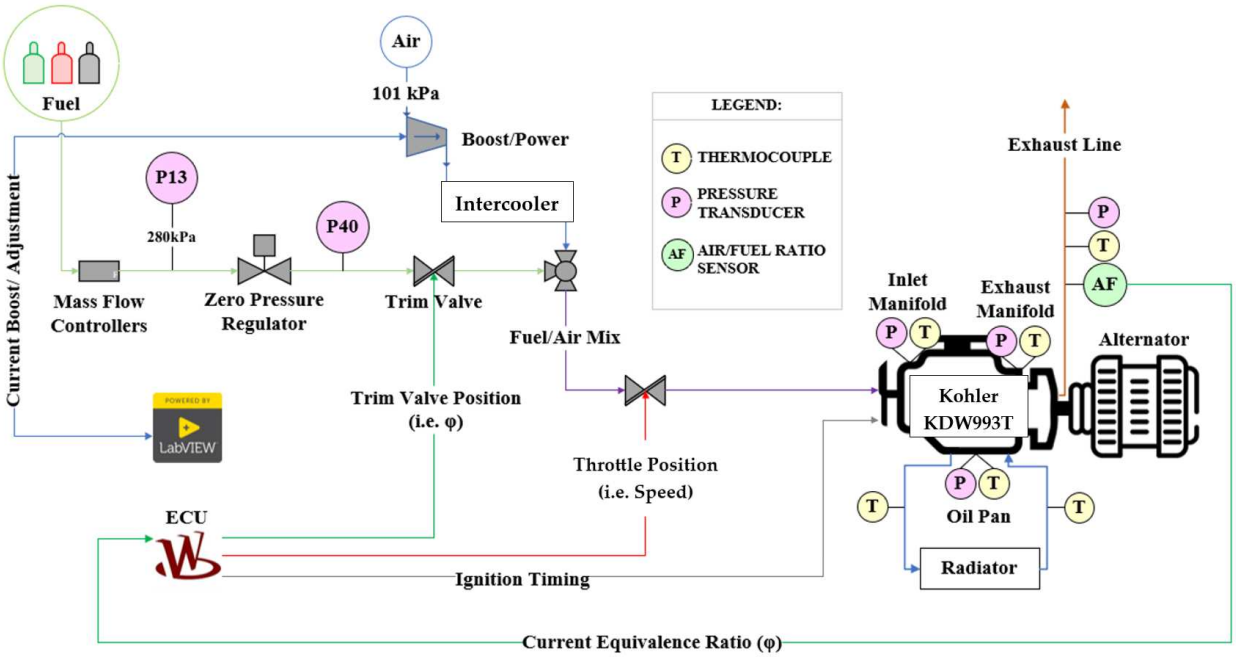

Figure 6. Facility diagram and engine controls.

The experimental engine is located at the CSU Powerhouse Energy Campus and is part of a larger SOFC-ICE hybrid power generation system. The facility consists of a modified diesel engine, a supercharger, an alternator, and a load bank. The load bank was used to simulate the expected power output for each fuel composition, based on their respective LHV, fuel flow rate, and alternator efficiency.

The fuel delivery was controlled by bottled gases that were blended together using mass flow controllers (DPCS-010392) to meet the different anode gas compositions. The fuel blends

consist of CO, CO2, H2, CH4, steam, and N2 at different amounts depending on SOFC load and fuel utilization. These compositions also have water as part of their constituents, but it is assumed to have been mostly removed by a water dropout heat exchanger to a dewpoint of 40°C. After the mass flow controllers, the fuel passes through a zero-pressure regulator to bias the fuel pressure to the air pressure. The engine control unit (ECU) then controls a trim valve to regulate fuel flow into the mixing valve, where air and fuel are mixed before entering the engine. Finally, the ECU adjusts the throttle to regulate engine speed to maintain steady-state operation.

3.2 Engine Control Unit Replacement

The ECU used in previous CSU research (OpenECU M220) shown in Figure 7a was replaced for this project. The original unit, coded by a Kohler Power Systems engineer, lacked the necessary documentation to modify its code to support the planned testing campaign as it used a complex algorithm to determine cam and crank synchronization from the manifold absolute pressure sensor. Also, the lack of knowledge and complex user interface for the ECU software, Vector CANape, made the troubleshooting process difficult. The new ECU chosen for the project was the Woodward SECM70, shown in Figure 7b. The advantages of switching to the SECM70 include local technical support for addressing any challenges, the ability to develop and document the ECU wiring harness and its sensors from the ground up, as well as its capabilities and software. A cam sensor shown in Figure 8 had to be installed on the engine for the ECU to substitute the algorithm previously used for crank and cam synchronization. Being a closed platform, Woodward provided its property PG+ software to control the ECU and also developed the initial calibration based on the engine geometry. For engine operation Appendix C shows the software tools used.

(**a**)

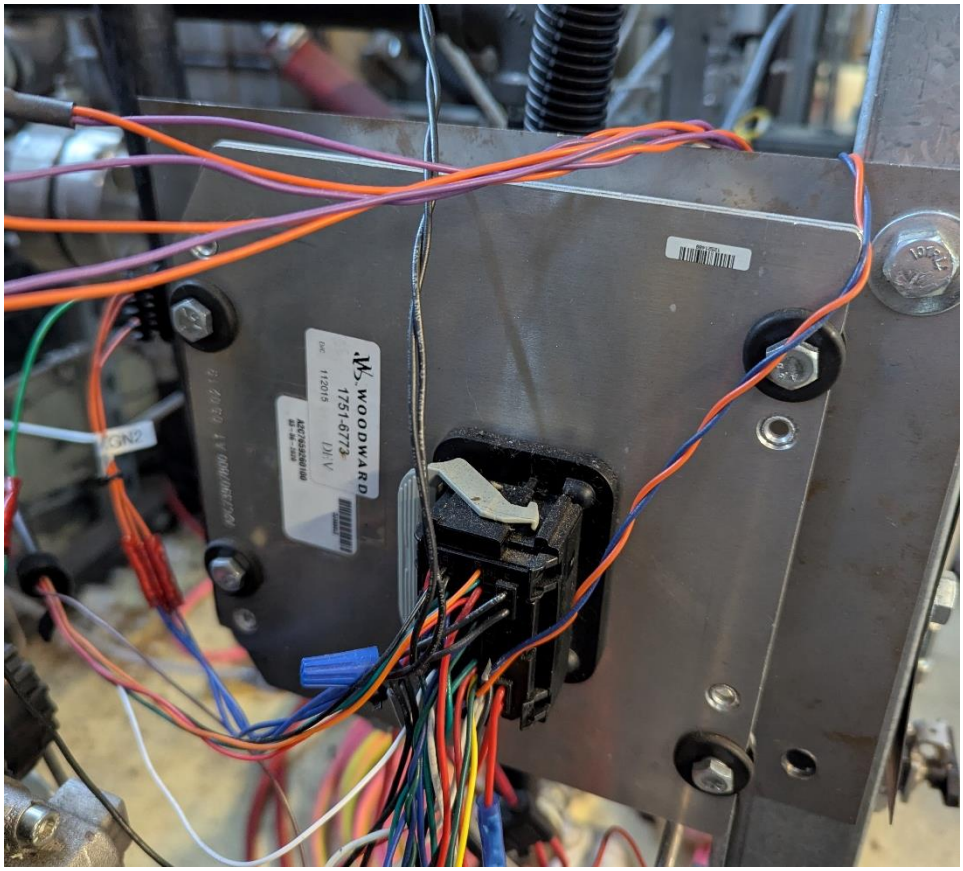

(**b**)

Figure 7. (**a**) OpenECU M220 , (**b**) Woodward SECM70

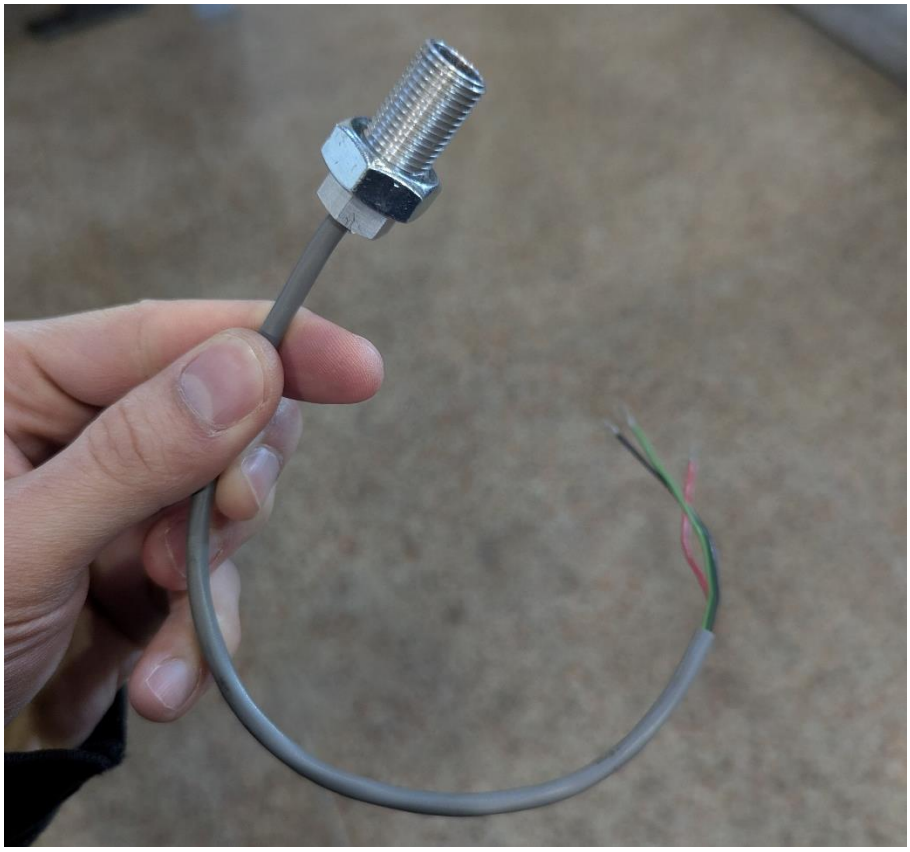

Figure 8. MSD Hall Effect Cam Sync Sensor

A closed loop system was used for real time performance adjustments based on the engine sensors. The benefit of using a closed loop system was the engine's ability to react to the fuel system that was decoupled from ECU. Also, equivalence ratio adjustments would happen automatically based on the air fuel ratio sensor, trim valve position, and throttle position. The other features used for testing were setting a target speed, target equivalence ratio and changing ignition timing. To monitor engine operation, a trend plotting graph was used.

3.3 Engine

The engine portion of the test facility consists of a 1.0-liter, 3-cylinder, Kohler diesel engine (KDW993T) modified for spark ignition. Figure 9 shows the engine skid inside the facility.

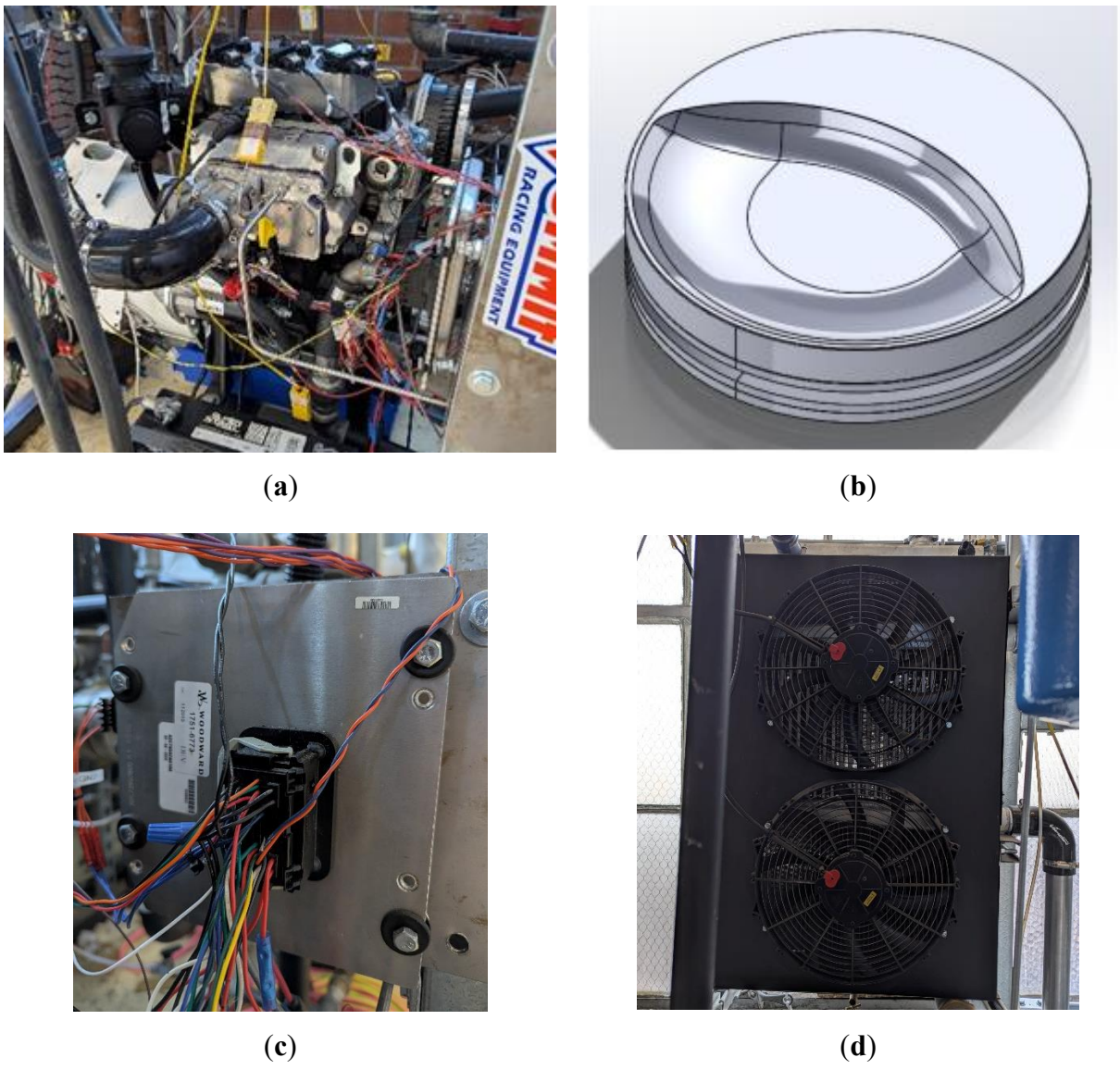

(**a**) (**b**)

(**c**) (**d**)

Figure 9. (**a**) Engine test skid, (**b**) 17:1 piston geometry, (**c**) ECU and (**d**) cooling system.

There were several engine modifications to convert the engine from CI to SI. These modifications involved adding spark plugs, as well as altering the piston geometry and engine controls. The reason for using a modifying a diesel engine was to enhance its durability. Diesel engines are typically made of stronger materials to handle higher compression ratios, making them a more resilient platform to the embrittlement effects of H2 combustion [46–48]. In addition, the piston geometry had to change to achieve the desired compression ratios with the SI modification. All modifications were first modeled and simulated using the engine modeling software GT-Power by researcher Valles Castro at CSU before being implemented [45]. Additional work for engine validation was conducted by researcher Countie, who focused on the predictive design and testing of the same platform [44]. The data collected contributed to determining the specifications shown in Table 3.

Table 3. Specification of a SI modified diesel engine.

Kohler KDW993T	
Bore	73.7 mm
Stroke	77.6 mm
Displacement	993 cc
Connecting rod length	0.1265 m
Compression ratio	17:1
Engine speed	1600 rpm

3.4 Supercharger

The supercharger used for testing was the Air Squared P24H056A-BLDC scroll compressor. Figure 10 shows the supercharger in the facility.

Figure 10. Air Squared P24H056A-BLDC supercharger.

The unit was used to boost the air going into the engine to meet the power requirements. As a parasitic load to the engine, the supercharger speed should be minimized to reduce electrical losses. However, if the boosted air is too low, the engine could deviate from steady state operation. Achieving a balance between boost and power is essential for reliable supplemental power generation.

3.5 Alternator

The alternator used for testing was the Kohler GC74037 and a WANPTEK KPS3010DF power supply as its exciter as shown in Figure 11.

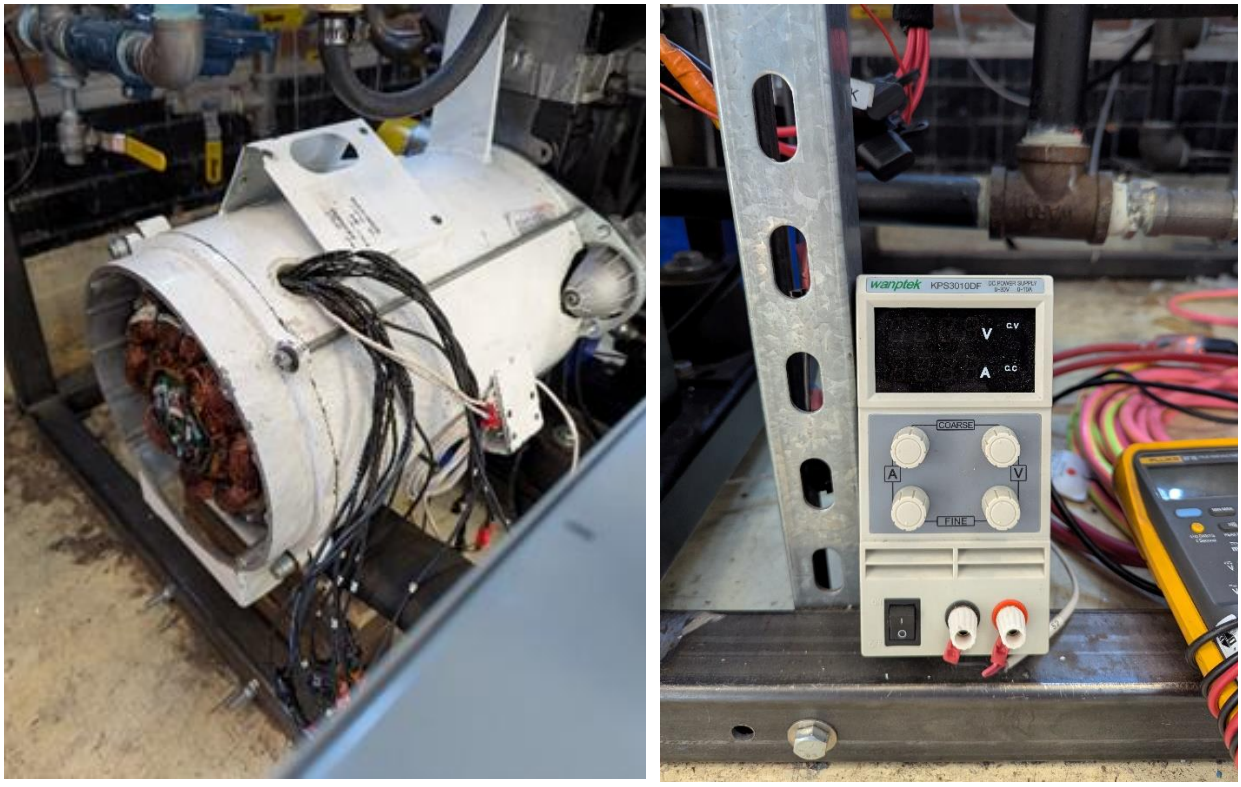

(**a**) (**b**)

Figure 11. (**a**) Kohler Alternator, (**b**) and exciter

The method of loading the engine is through an alternator and load bank. The alternator efficiency, shown in Figure 12 was provided by Kohler Power Systems.

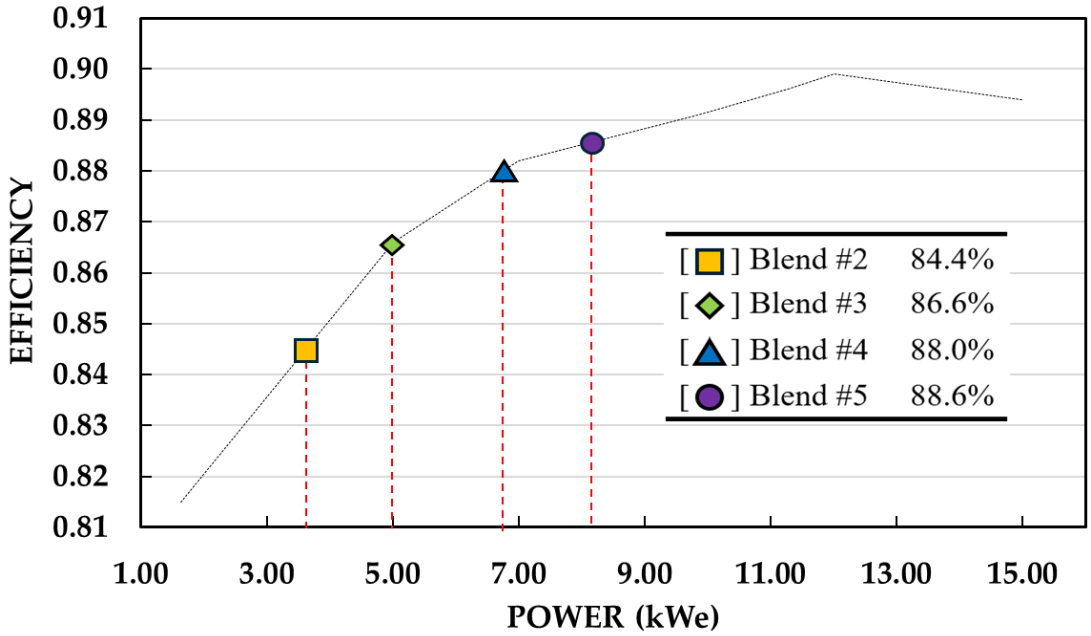

Figure 12. Calibrated alternator performance data provided by Kohler Power Systems.

The primary detail to note from this figure was that the alternator efficiency varied with changes in power output. For this reason, the generator efficiency used in the BTE calculations had to change depending on the fuel blend. Additionally, the exciter was held constant at ~ 11.3V and 2A throughout testing to only record the effects of fuel composition in power generation.

3.6 Load Bank and Emissions

The last component used for testing was LCNFM1 load bank. This device was used to apply torque to the engine through the alternator at the expected electrical power output for each blend. The Fluke-1732/B energy logger monitored and averaged the power output from the load bank. This setup ensured a constant engine load while other parameters were adjusted during testing to observe their impact on engine performance. Figure 13 shows the load bank and the energy logger used for testing.

(**a**) (**b**)

Figure 13. (a) LCNFM1 load bank, (b) Fluke-1732/B energy logger

Emissions measurement samples were collected via an exhaust sample port and directed through a heated sample line into a control room equipped with the necessary instrumentation for exhaust gas analysis. The analytical methods used during testing included Fourier Transform Infrared (FTIR) spectroscopy and a Five-gas analyzer. Each combustion strategy serves a specific purpose: FTIR focuses on wet emission analysis, while the five-gas analyzer measures dry emissions [49].

3.7 Software

Figure 14 shows the five software programs utilized during testing. LabVIEW (2020 SP1) was used for managing supercharger speed and fuel delivery, PG+ (v43.11) for controlling the ECU and logging engine sensor data, Microsoft 365 (16.0.16529.20182) for data analysis, Engineering Equation Solver (EES) for uncertainty propagation, and Python Spyder (6.0.0) for averaging the raw data. All programs and codes used are available, except for PG+, which is proprietary software developed by Woodward and is not readily accessible. The next section will explain the testing methodology, including data acquisition, testing and analysis approach.

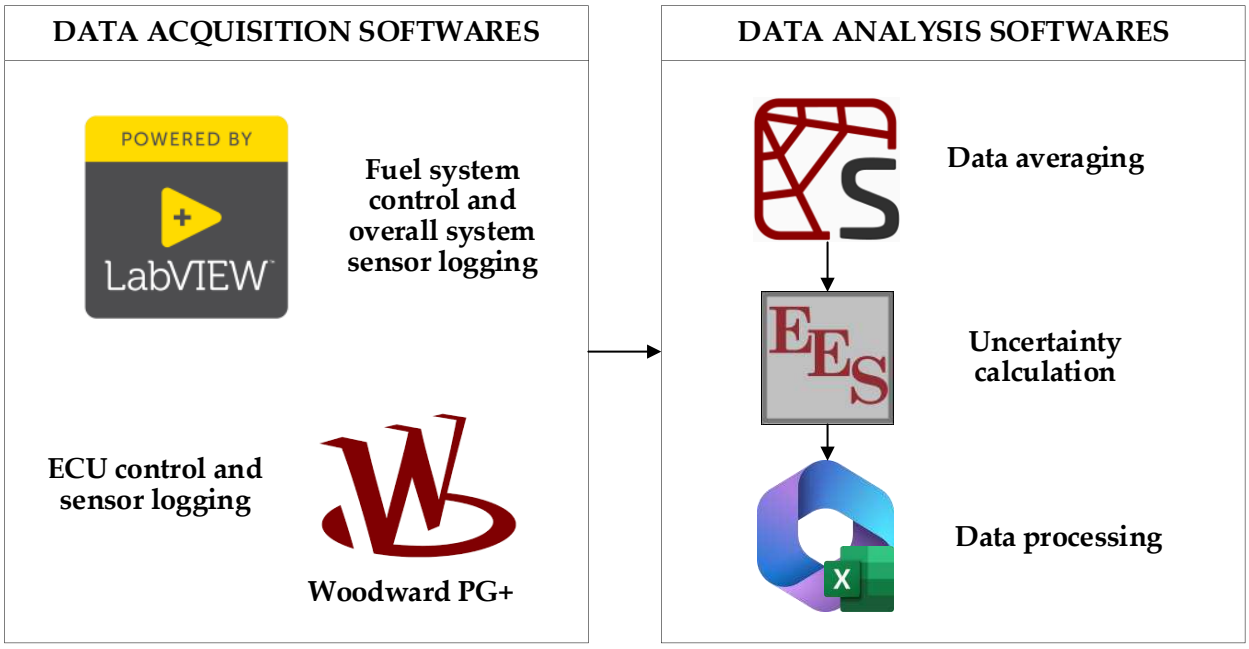

Figure 14. Program utilization flowchart

CHAPTER 4. METHODOLOGY

4.1 SOFC Model Data

The testing methods were based on the fuel composition as shown in Table 4. The "Legacy fuel composition" refers to a fuel blend used in previous studies at CSU, based on an earlier SOFC model developed by the Colorado School of Mines. The "New fuel compositions" category includes all the anode gas blends anticipated for use with the engine, based on the current SOFC model [50]. The fuel blends target LHV (LHV_f) shown in Table 4 were calculated utilizing the following equations:

$$X_i = \frac{\#\ moles_i}{total\ moles} \tag{1}$$

$$MW_f = \sum MW_i * X_i \tag{2}$$

$$Y_i = X_i * \left(\frac{MW_i}{MW_f}\right) \tag{3}$$

$$LHV_f = \sum LHV_i * Y_i \tag{4}$$

where X_i, Y_i, MW_i, and LHV_i are the mole fractions, mass fractions, molar weights, and LHV of the constituents, respectively, while MW_f is the molar weight of the fuel blend. Using these LHV_f

values it is possible to calculate the expected power for each fuel composition using the following equation solved for W_e:

$$BTE = \frac{W_e/\eta_g}{m_f * LHV_f} \quad (5)$$

where the BTE target was assumed to be 35% [44], η_g is the corresponding alternator efficiency for each blend, and the target fuel mass flow rate m_f is shown in Table 4 under "Flow rate [g/s]". With the model data and calculated LHV_f, a consistent testing methodology was produced to test the engine at all the expected operational conditions and optimize for best performance. It is also important to note that the LHV_f used for all BTE calculations was calculated from flow rate of each fuel constituent measured by the mass flow controllers during testing. The LHV_f and flow rates m_f shown in Table 4 were target values. This was considered during the uncertainty propagation calculations.

Table 4. System model outputs for anode tail gas fuel compositions at different SOFC utilizations.

SOFC Load	Flow rate [g/s]	LHV_f [kJ/kg]	Composition [mol %]						$\dot{W}_e$ [kW]	SOFC-ICE Power [kW]
			CO	CO_2	CH_4	H_2	H_2O	N_2		
Legacy fuel composition:										
Blend 1	7.93	4047	9.3	53.8	0.76	33.6	2.5	0.3	~10	80
New fuel compositions:										
Blend 2 (50% load)	3.60	3328	6.7	60.3	1.6	28.5	2.4	0.3	3.56	40
Blend 3 (75% load)	4.98	3382	7.9	58.9	1.0	29.3	2.5	0.3	5.01	60
Blend 4 (100% load)	6.80	3356	8.0	59.3	1.2	28.5	2.5	0.3	6.79	80

Blend 5 (125% load)	8.47	3267	8.0	60.1	1.3	27.6	2.6	0.3	8.23	100

For this research, the steam was replaced with CO_2 since both gases served the same purpose of diluting the fuel. Prior research conducted at CSU showed the engine's performance metrics when steam was dropped out and a small volume of water was utilized as part of the fuel blend [51–53]. Therefore, for ease of testing, CO_2 was used instead of steam and N_2 was neglected because of its small amount.

4.2 Legacy Data

To develop a consistent testing methodology, engine conditions were chosen as a baseline. The specifications shown in Table 3 were based on engine geometry and previous testing done with the same engine platform [54], but the equivalence ratio (φ) was chosen based on the data shown in Figure 15. This data was acquired in 2022 for the same engine model and configuration running on Blend 1 as shown in Table 4. As previously stated, this fuel is based on an older SOFC anode gas compositions and load target based on earlier system modeling than the blends that will be optimized in this research. During the test campaign on Blend 1, an ignition and equivalence ratio sweep were done to find the optimal points for each parameter. The highest efficiency calculated was obtained with an $\varphi = 0.70$ showing a BTE of 36.3%, while the ignition timing sweep showed a maximum BTE of 36.0% with $\varphi = 0.75$, both at 40° BTDC and 10kW of load. Based on this previous research, the chosen equivalence ratio for the new tests was 0.75 because of three main factors: efficiency stability, supercharger requirements, and fuel LHV. With a $\varphi = 0.70$ the engine may have hit its maximum BTE, but as seen in Figure 15b, there was a substantial drop off in efficiency when going from $\varphi = 0.70$ to 0.65. To avoid this efficiency boundary, a $\varphi = 0.75$ was selected because it has a similar efficiency but has less risk of deviation in case of an

unexpected operational changes. Additionally, running at lower equivalence ratio would require the supercharger to run at higher speeds, increasing the parasitic loads and reducing overall system efficiency. Moreover, the new fuel blends have a lower LHV than the legacy fuel blend. Having a lower LHV could change the mixing requirements of the fuel blends, requiring more fuel to be mixed with air for combustion [55]. These factors made an φ = 0.75 more suitable for the engine to sustain high efficiency over a bigger range of conditions. The difference between BTEs was < 1%, which is within the uncertainty of the measurement. The torque measurement from this legacy testing was measured with a dynamometer, so the BTE was calculated using the following equation:

$$BTE = \frac{\tau_{\text{Brake}} * N / 9548.8}{m_{\text{f}} * LHV_{\text{f}}} \tag{6}$$

where τ_{Brake} is the engine torque in N*m and N is engine speed in RPM.

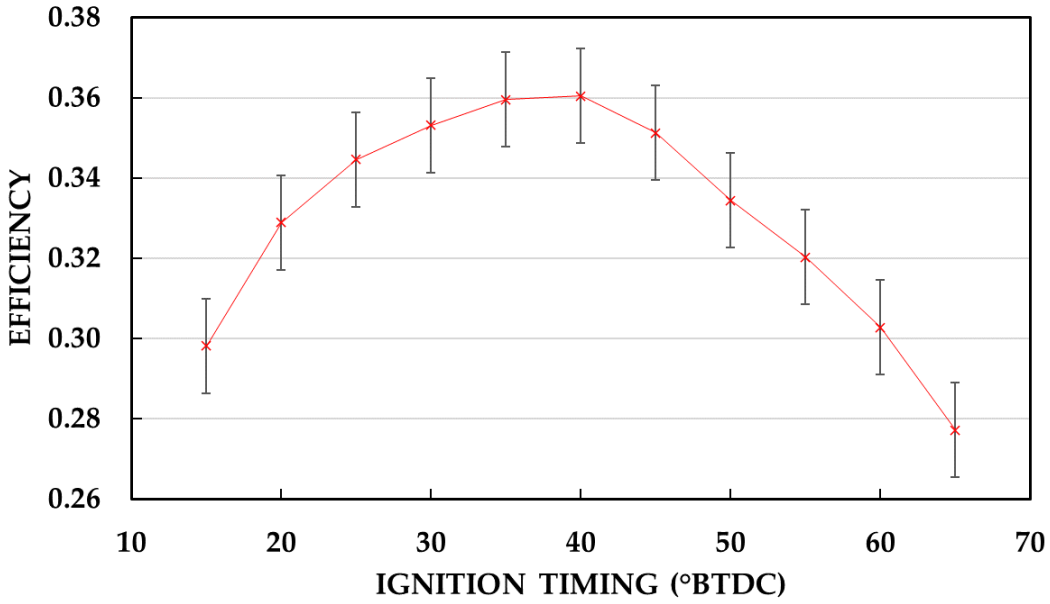

(a)

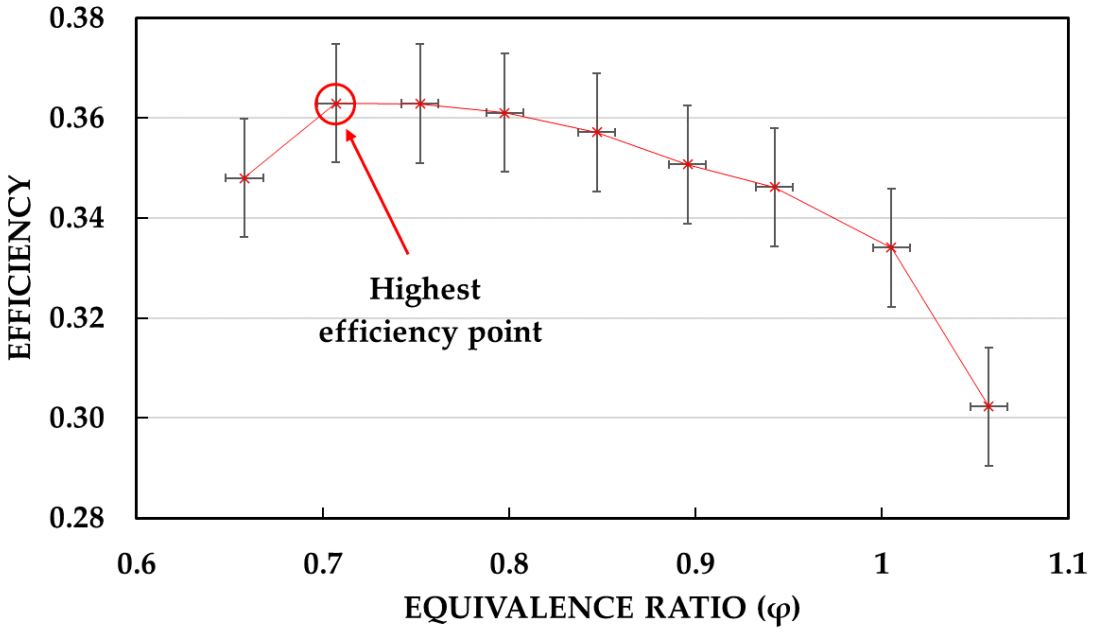

(**b**)

Figure 15. **(a)** Blend #1 ignition timing sweep to determine the best crank angle degree (CAD) of spark to achieve maximum BTE. Testing showed a maximum BTE of **36.0%** at these conditions: **40° BTDC, 0.75Phi, 150kPa, 10kW load. (b)** Blend #1 equivalence ratio sweep to determine best air-fuel ratio to achieve maximum BTE. Testing showed a maximum BTE of **36.3%** at these conditions: **40° BTDC, 0.70Phi, 158kPa, 10kW load** [54].

4.3 Testing Approach

4.3.1 Ignition Timing Sweep

The testing program evaluated for Blends 2-5 in Table 4 began with an ignition timing sweep from 30° BTDC to 60° BTDC for each blend while holding power constant. Ignition timing was increased in increments of 5°, having a total of seven test points for each fuel. For validation purposes, a timing light was used to ensure that the values stated by the ECU software were accurate to the real timing. To ensure that all test points were recorded at the same condition, engine speed and equivalence ratio were held constant at 1600 rpm and 0.75 respectively. If the engine speed did not meet 1600 rpm at any of the ignition timings, the supercharger speed was

changed to reach steady engine speed. The power applied via the load bank stayed constant during the test to observe the effects of ignition timing on the mass flow rate of the fuel. The data was analyzed to determine the optimal ignition timing that yielded the highest efficiency for each fuel blend. The results were then compared to Figure 15 to assess the impact of the fuel's LHV and load.

4.3.2 Supercharger Boost Sweep

In addition, boost was swept by varying the supercharger speed for a fixed fuel flow and power level. The goal was to find the range at which the supercharger could be run to maintain steady state. Environmental conditions, such as ambient air temperature, could change during operation, directly affecting engine performance. Establishing the operational range of the supercharger for each blend would ensure that the engine performs at steady state, regardless of environmental changes. More importantly, the boost sweep determined the lowest air pressure required to operate the engine at each blend which reduces the supercharger's electricity consumption and increases the overall hybrid system efficiency.

4.3.3 Emission Measurements

A lean combustion reaction was solved for all the gas blends to provide an estimate of combustion product concentrations.

$$C_{\mathrm{x}}H_{\mathrm{y}}O_{\mathrm{z}} + a(O_2 + 3.76N_2) \rightarrow bCO_2 + dH_2O + fO_2 + 3.76(a)N_2 \quad (7)$$

By comparing the measured combustion products to the calculated values, the composition of the emission samples could be estimated, ensuring they accurately represented the exhaust gases from the engine. For FTIR data, the combustion product used for estimation was water content in the sample. Comparing the real water content to the expected water percentage of a perfect

combustion would ensure that the sample was within the expected range. The same process was applied to Five-gas, but the combustion product for estimation was oxygen percentage.

4.3.4 Speed Sweep

Blend 4 was chosen as the fuel composition to test during the speed sweep since the LHV between the new blends were similar and this fuel would be the one most available during system operation. Speed range selected for the tests was from 1400 rpm to 1800 rpm. During testing, the load was held constant at its expected power output to see the effects that speed would have on efficiency. However, ignition timing and boost were changed to achieve steady state operation. The results of the engine test program were the operational conditions for the engine to achieve maximum power output and are shown in the following section.

4.4 Uncertainty Calculations

The uncertainties of the instruments used during testing were applied to determine the uncertainty of each calculated parameter. For the ignition timing sweep, both the mass flow controllers and the energy logger data sheets were considered. The mass flow controllers had an uncertainty of ±0.002 for full-scale measurements and ±0.005 for mass flow readings, while the energy logger had a 1.2% uncertainty for power readings. In the boost sweep, the current clamp used to calculate power consumption had an uncertainty of ±3.0% of the reading plus 10 digits as stated on the data sheet. Lastly, the five-gas analyzer data sheet had an uncertainty of 1% of full scale measurement for all constituents. These uncertainties were factored into all calculations to assess error propagation.

CHAPTER 5. RESULTS AND DISCUSSION

5.1 Ignition Timing Sweep

The initial optimization results to be discussed are from the ignition timing sweep, as illustrated in Figure 16. The data showed an increase in BTE when going from the lowest to the highest load blend. The maximum efficiency recorded for each blend was 23.6% for Blend 2 at 55° BTDC at 3.29kW, 27.1% for Blend 3 at 5.01kW, 29.6% for Blend 4 at 6.81kW, and 31.0% for Blend 5 at 8.17kW, all at a timing of 50° BTDC. The increase in efficiency was anticipated because the power production for the blends was increasing so the parasitic loads of the engine were a lower fraction of the total power produced at higher output powers. These parasitic loads include frictional losses, pumping losses and supercharger power consumption. It is worth mentioning that during the ignition timing sweep, although the supercharged air passed through an air-coupled heat exchanger, the initial intake air temperature increased throughout the test day. The temperature for Blends 2 to 4 began at approximately 30°C and increased to 34°C, while for Blend 5, the intake temperature started at 32°C and reached 39°C. These increases in temperature were primarily caused by an increased ambient temperature throughout the test day. For Blends 2 to 4, the ambient air temperature increased from 26°C to 29°C, while Blend 5 started at 32°C and ended at 39°C. This could have affected the BTE since a lower air temperature would have benefited engine performance [56].

The data from Blends 2 - 5 show a decrease in efficiency as compared with the legacy blend. This could have been because the LHV of Blend 1 was 13% higher than the highest LHV among the new blends, along with a higher load. Dropping the LHV at the same equivalence ratio

and boost would directly affect the power being produced. To increase power production a higher boost would be required, but this would increase parasitic loads. In contrast, a higher LHV would increase the thermal energy produced by combustion, generating more power. Additionally, the reduced load contributed to the decrease in BTE compared to the legacy blend. The results from the new blends are still deemed satisfactory, as a 4% reduction in the engine's maximum efficiency corresponds to only a 1% decrease in the overall system's efficiency, making it a minimal change.

All the blends achieved a maximum BTE at 50° BTDC, except Blend 2 which was at 55° BTDC. The advanced timing could be due to the low hydrogen and high CO2 content in the blend, which makes the fuel more dilute and less reactive. Regardless, it was still recommended to use 50° for all blends since the difference in BTE between 50° to 55° was < 1%. This would simplify engine controls by keeping the ignition timing the same at every SOFC fuel utilization. A similar explanation to the one for Blend 2 can be applied when comparing the optimized timings to those used during Blend 1 testing. The higher hydrogen concentration in Blend 1, relative to the new blends, may have contributed to the 10° difference in spark timing.

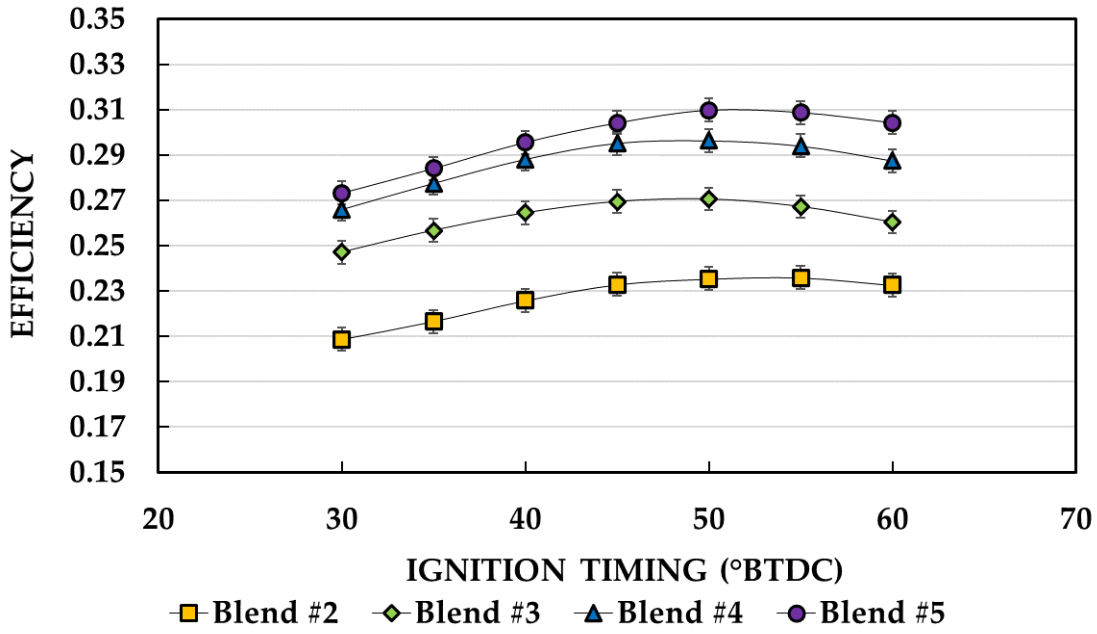

Figure 16. Ignition timing sweep to determine the best CAD of spark to achieve maximum BTE at the following **steady state conditions**: 1600rpm, 0.75phi. Maximum BTE was achieved at these spark timings: **Blend #2**: 23.6% at 55° BTDC with 3.29kW power output, **Blend #3**: 27.1% at 50° BTDC with 5.01kW power output, **Blend #4**: 29.6% at 50° BTDC with 6.81kW power output, **Blend #5**: 31.0% at 50° BTDC with 8.17kW power output.

5.2 Supercharger Boost Sweep

The boost sweep followed a similar procedure to the ignition timing tests. During the boost sweep, all other parameters except the supercharger speed were held constant and the ignition timings were set to the values discovered during the timing sweep. Figure 17 shows the boost range for each blend in which steady state conditions could be met with the throttle controlling engine speed. The upper limit was defined as the maximum boost the engine could receive while still holding constant speed. In contrast, the lower limit was the minimum boost required for the engine to reach the target speed. These limits were based on the throttle position during testing. The throttle movement range during operation was from 2% to 23%. The limited movement for the throttle body occurred because of the equivalence ratio and flow restriction. Even though the trim

valve is the one in charge of equivalence ratio, as shown in Figure 6, the throttle still had an effect. This relationship was mainly caused by the engine's fuel delivery system. The engine air side flowed directly from the supercharger to the mixing valve and then into the intake. In addition, the fuel side had to pass through the mass flow controller, the regulators, and the trim valve before reaching the mixing valve and finally the intake. Since the fuel delivery was much slower than the air side, if the throttle opened more than 23% the equivalence ratio would reduce lower than 0.75, deviating from steady state conditions. Therefore, the supercharger speed at which the throttle was nearest to 2% was called upper limit, while the lower limit was the boost speed at which the throttle was nearest to 23%. Testing showed that the lower limit was the most optimal because it lowered the power consumption from the supercharger and slightly increased efficiency. The BTE was calculated for the lowest boost value and the results indicated a 1% efficiency reduction for Blend 2, while Blends 3-5 showed an average of 1% increase in efficiency compared to the ignition timing sweep. The less restrictive throttle position may have improved fuel distribution to the engine, enhancing combustion efficiency. This could also explain why, in nearly all cases where the inlet manifold pressure and boosted pressure were the same, the engine achieved the highest BTE. In contrast, the reduction in BTE for Blend 2 could have been influenced by environmental conditions. While testing conditions were nearly identical on both test days, ambient air temperature differed. This is why it's important to highlight that inlet manifold and ambient air temperatures changed significantly during the boost sweep. During testing with Blends 2 and 3, the intake temperature started at 41°C and rose to 42°C, while the ambient temperature increased from 34°C to 36°C. For Blends 4 and 5, the intake temperature began at 38°C and reached 41°C, with the ambient temperature changing from 31°C to 32°C. As previously mentioned, the difference in intake temperature compared to the ignition timing sweep could have affected the

newly calculated BTE. Nonetheless, testing showed that efficiencies could be increased with optimal boost pressure, reaching as high as 31.4%, even in less than favorable temperature conditions. This could have meant that if temperatures had been constant during both tests, an additional estimate of 1% higher BTE could have been achieved. Also, the lower limit boost would benefit the overall system efficiency by reducing the power being consumed by the supercharger.

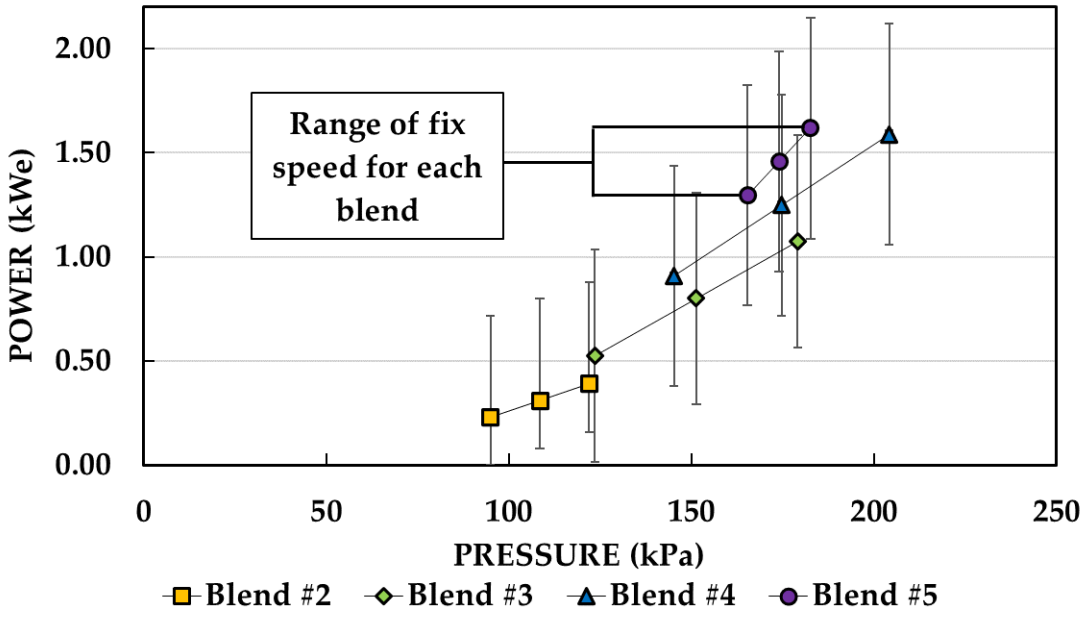

Figure 17. Boost sweep to determine the range of operation at which **steady state conditions** are met (1600rpm, 0.75phi). Results showed a maximum BTE of 31.4%. It was found that **lower limit** conditions are the **most beneficial** for engine performance, with an **average increase of 1% BTE**, and most power savings.

5.3 Ignition Timing Sweep with Parasitic Losses

After completing both the ignition and boost sweeps, the data sets were combined to assess the impact of the supercharger on the engine's BTE. The ignition timing data was used in conjunction with the power consumed by the supercharger at the lower limit subtracted from the engine's total power output. Figure 18 illustrates the engine's BTE including parasitic losses.

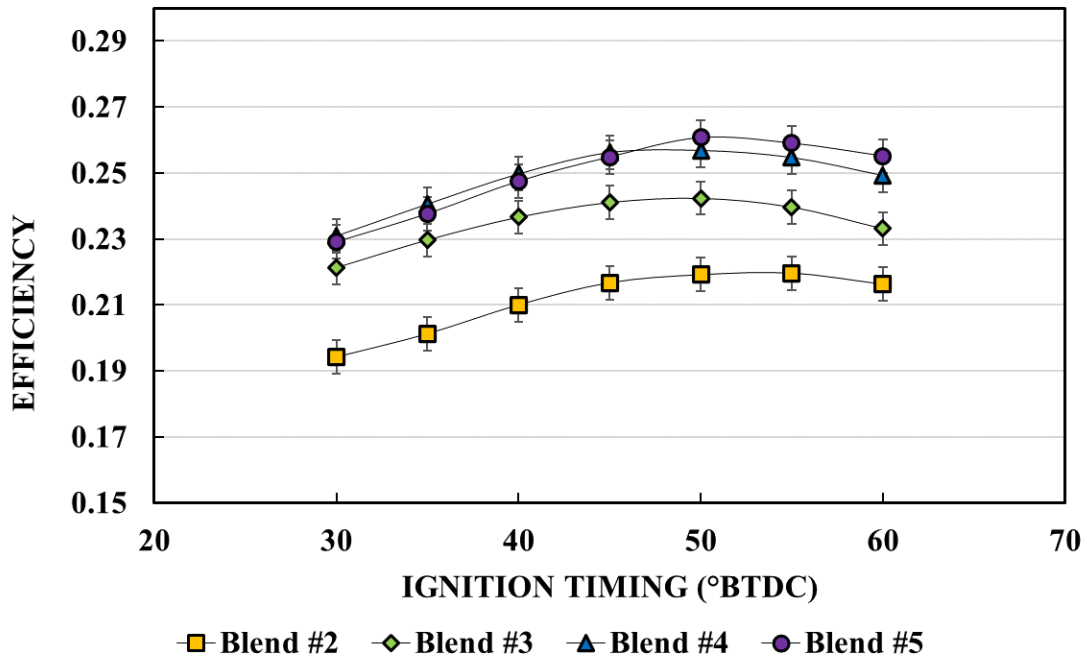

Figure 18. Ignition timing sweep to determine the best CAD of spark to achieve maximum BTE at the following **steady state conditions**: 1600rpm, 0.75phi. Maximum BTE was achieved at these spark timings: **Blend #2**: 22.0% at 55° BTDC with 3.06kW power output, **Blend #3**: 24.2% at 50° BTDC with 4.49kW power output, **Blend #4**: 25.7% at 50° BTDC with 5.90kW power output, **Blend #5**: 26.1% at 50° BTDC with 6.87kW power output.

The results show a reduction in BTE corresponding to an increase in power output. The maximum efficiency recorded for each blend was 22.0% for Blend 2 at 55° BTDC at 3.06kW, 24.2% for Blend 3 at 4.49kW, 25.7% for Blend 4 at 5.90kW, and 26.1% for Blend 5 at 6.87kW, all at a timing of 50° BTDC. This is expected, as higher power demands require more boost, which in turn increases the electricity consumption of the supercharger. Another key observation is the overlapping efficiency between Blend 4 and Blend 5. This suggests that there may be a point of diminishing returns with the engine's power output. If the engine were to operate under higher loads with these fuel blends, the increased supercharger energy consumption would eventually offset any gains in engine power, resulting in little to no improvement in overall system efficiency.

Moreover, this analysis assumes a best-case scenario, as the upper limit of supercharger could lead to even more reductions to engine's efficiency.

5.4 Emission Measurements

5.4.1 FTIR Data

The next phase of testing was the emissions. All samples were taken by using the optimized timings and boost conditions from the previous tests. After comparing the calculations with the emission samples, it was noted that the FTIR data was unreliable because of human error. Appendix B shows more details regarding emissions data. When comparing the complete combustion H2O content with the FTIR results, it was observed that the expected water content for all blends was ~ 4.5%, but the FTIR readings consistently showed 0 % for all measurements. Additionally, total hydrocarbons (THC) and CO emissions also differed substantially from previous work done with Blend 1 [44]. This could have been caused by the sample being taken too far from the engine's exhaust tubing, causing the water content to condense out of the sample, changing the composition. The other possibility for this inaccuracy could have been an uncalibrated or defective instrument.

5.4.2 Five-gas Data

In contrast, Five-gas showed more realistic data compared to the lean combustion reaction results. A detailed description of Five-gas analyzer used in this testing is referenced in King [57]. All the necessary data to calculate BTE was also recorded and analyzed to ensure that the engine performance was the same as previous tests. Figure 19 shows the emissions results as brake specific emissions, a standardized industry technique to normalize the emissions based on engine power. The three metrics which were analyzed were brake specific total hydrocarbons (BSTHC), brake specific carbon monoxide (BSCO), and brake specific nitrogen oxides (BSNOx) [58]. Blend

2 exhibited the highest BSTHC at 3.48 g/bkW-hr. In comparison, the other blends displayed a gradual increase in BSTHC, but their emissions remained lower than those of Blend 2. This may have been due to Blend 2 having the highest CH4 content out of all blends or by low combustion efficiency. As seen in Figure 16, Blend 2 also showed the highest BSCO with 37.2 g/bkW-hr. A lower BSCO indicates higher combustion efficiencies, which it's another possible explanation of why the BSTHC was much higher for Blend 2 compared to the other blends [44]. This low combustion could have been caused by Blend 2 being the more dilute out of all the fuel compositions. For Blends 3 - 5, the BSCO was similar across the different fuel compositions which indicates consistent combustion efficiency. The increase in BSTHC for these blends may be due to the methane content in each blend. As shown in Table 4, Blend 2 has the highest methane content, followed by Blend 5, Blend 4, and finally Blend 3. This pattern aligns perfectly with the BSTHC results from the emission measurements. The BSNOx results showed values close to zero which is likely caused by the lean fuel mixture and cold combustion. Typical engine exhaust temperatures can reach up to 850°C, whereas this engine peaked at approximately 372°C while delivering its maximum power output.

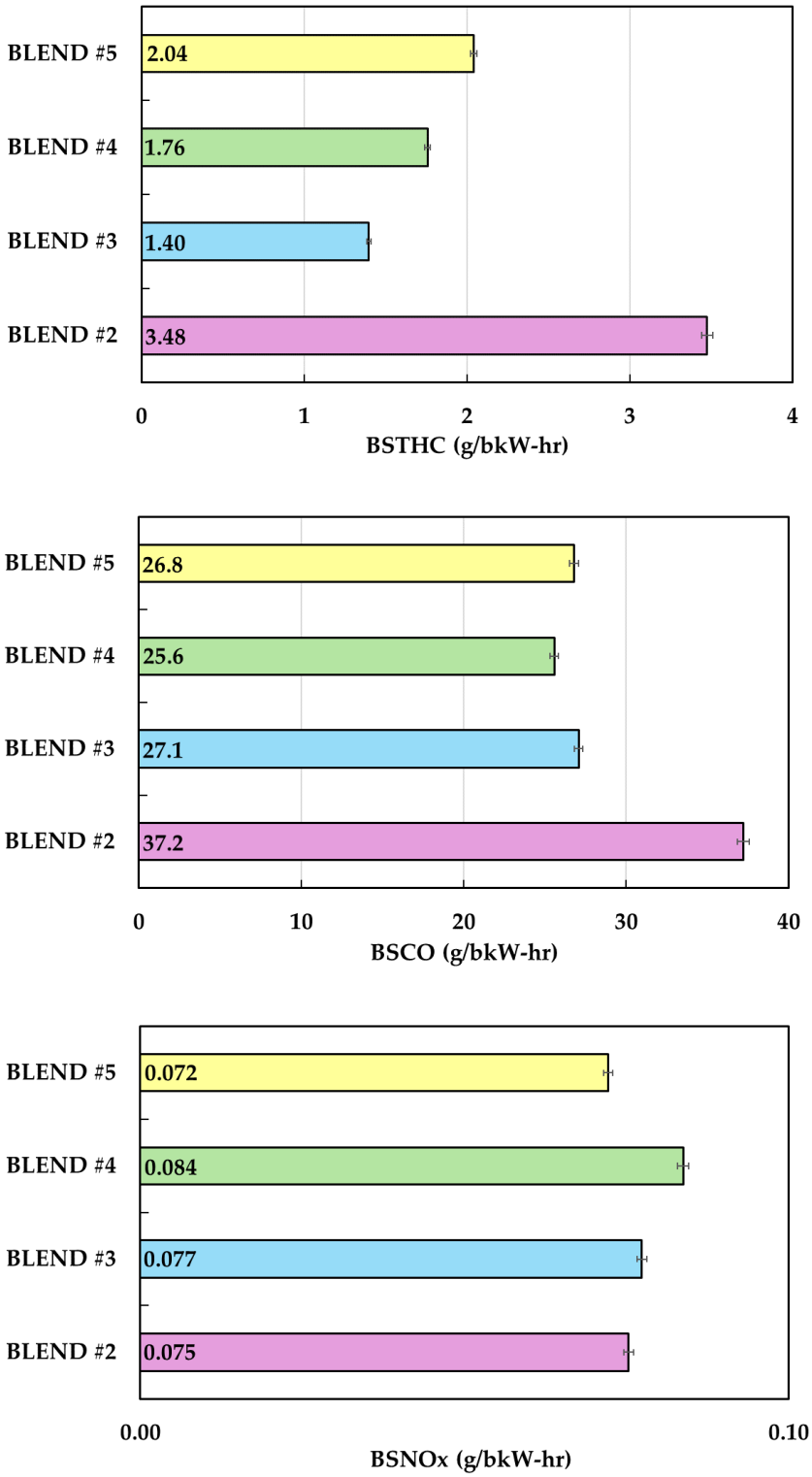

Figure 19. Brake specific emissions for all fuel blends tested using **Five-gas analyzer**. A catalytic coverter is required to meet the South Coast Air Quality Management District emission regulation.

The brake-specific emissions for the new fuel blends demonstrated a significant reduction in both BSCO and BSNOx compared to the legacy blend emissions shown in Table 5. This improvement could be attributed to changes in the fuel composition. When comparing the constituents of each blend in Table 4, Blend 1 stands out with the lowest CO2 percentage among all the blends. Lower CO2 content in the fuel generally leads to higher NOx production due to the reduced amount of diluent in the fuel. Additionally, the higher H2 content in the legacy blend could have raises the combustion temperature, which further contributes to increased NOx emissions.

Table 5. Brake specific emissions for legacy blend [44].

Engine Speed [RPM]	1600	1600	1800	1800
Ignition Timing [°BTDC]	16	23	17	26
Brake Specific THC [g/bkW-hr]	0.53	0.56	0.67	0.39
Brake Specific Carbon Monoxide [g/bkW-hr]	45.5	65.1	51.6	41.3
Brake Specific NOx [g/bkW-hr]	6.8	6.8	11.0	8.7

Regarding BSCO emissions, a lower value indicates better combustion efficiency. This suggests that the new blends, with their altered composition, improve combustion efficiency by nearly 50% compared to the legacy blend. Another possibility could be the increased concentration of CO from Blend 1 not getting fully combusted. The only emission that showed an increase relative to Blend 1 was BSTHC. This increase can likely be explained by the higher CH4 content in the new blends, which would elevate the total hydrocarbon (THC) emissions, subsequently raising the BSTHC.

As a standalone engine, emissions did not meet the legal requirements of 0.20 g/bkW-hr for BSTHC and BSNOx, and 0.80 g/bkW-hr for BSCO as mandated by the South Coast Air Quality

Management District [59]. However, when accounting for the total hybrid SOFC-ICE system power output (80 kW) and considering that these are the only emissions from the entire system, the legal requirements for new engines are met, except for the BSCO. Figure 20 displays the emissions of the overall system compared to the legal requirements for Blend #4. Therefore, a catalytic oxidizer at a minimum 63% CO oxidation is required to meet the BSCO legal emissions limits.

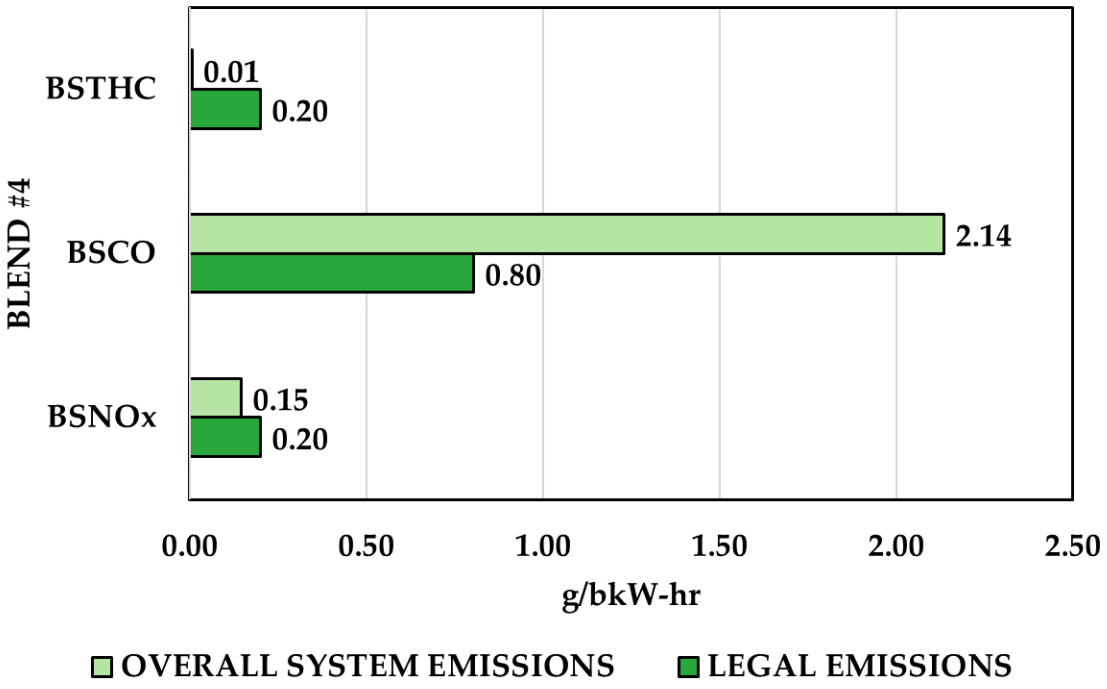

Figure 20. Overall system emissions compared to the legal requirements from the South Coast Air Quality Management District for new engines.

5.5 Speed Sweep & Operational Conditions

Figure 21 illustrates the results from the speed sweep, the last test within the scope of this research. The engine was operated at 1400 RPM, 1600 RPM, and 1800 RPM and the results indicate the highest efficiency occuring at 1600 RPM of approximately 29.9%. The reduction in efficiency for 1400 rpm could have been by increase frictional and pumping losses, while 1800

rpm showed a reduction because of the advance timing changing the cylinder dynamics off its design point. Therefore, it is reasonable to conclude that the reduction in the fuel's LHV and load compared to Blend 1 did not affect the optimal engine speed.

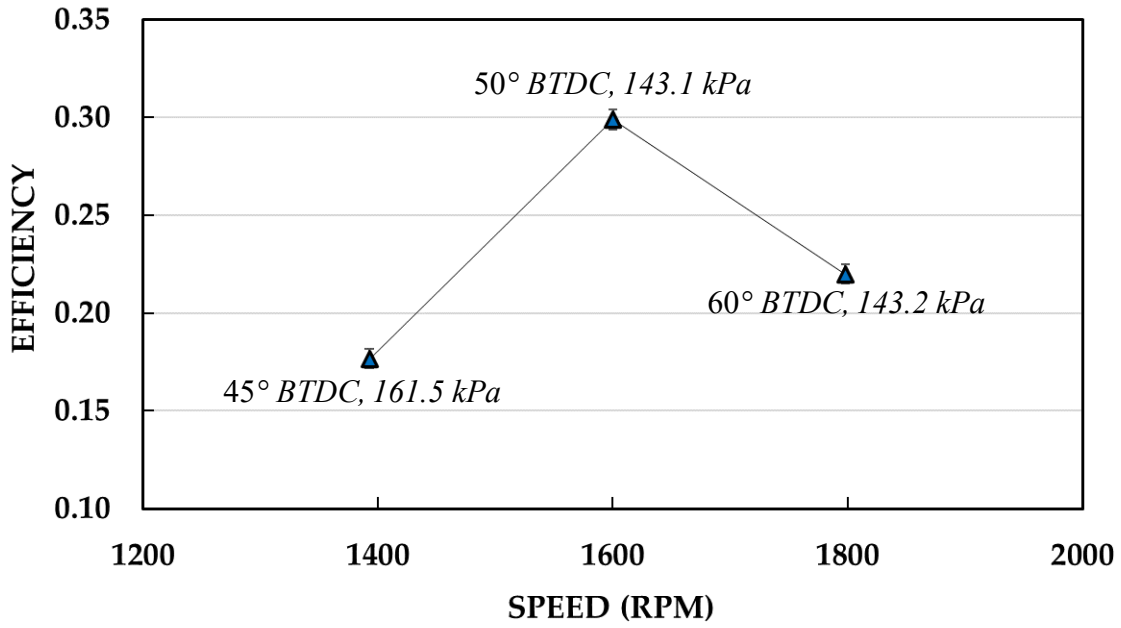

Figure 21. Speed sweep for **Blend #4** to determine the optimal engine speed to achieve maximum BTE. Testing showed that **1600 rpm** was the optimal speed for the **highest efficiency** at of 29.9%.

5.6 Operational Conditions

Maintaining steady-state conditions for the engine was crucial for reliable data acquisition. The primary objective of this research was to develop a control strategy for an engine running on anode gas. Analyzing the boost and mass flow behavior during startup, steady-state, and transient conditions across all fuel blends was key to understanding how to control the engine most effectively. Figure 22 illustrates the boost and mass flow behavior at these various stages.

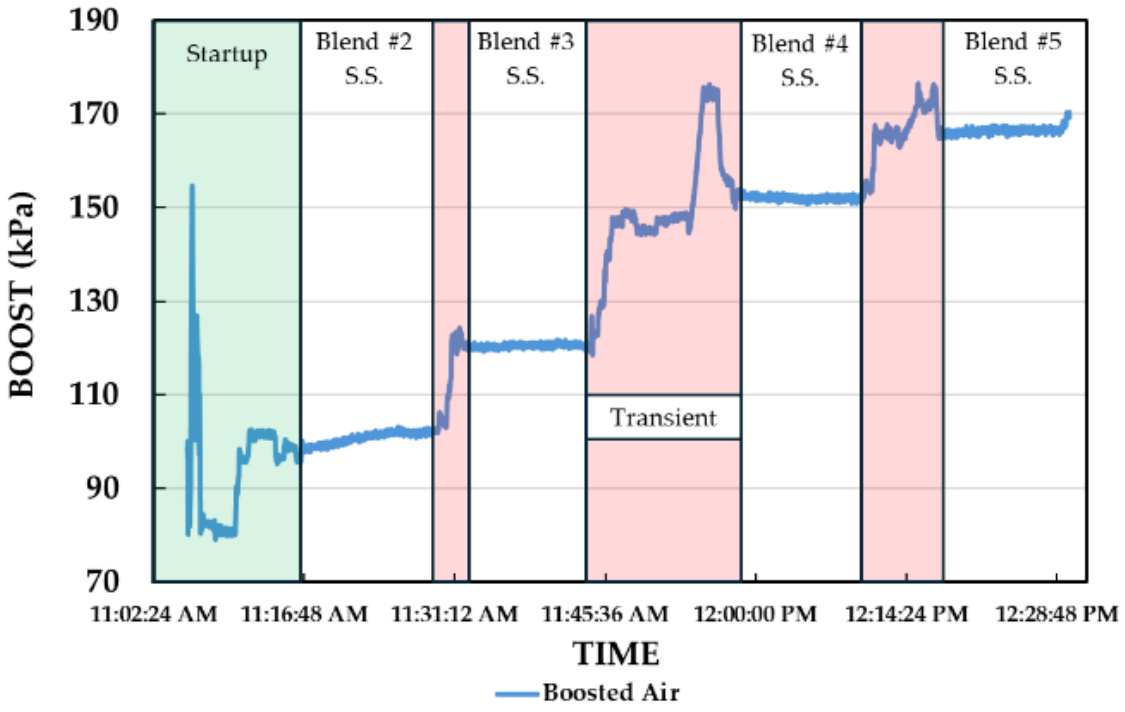

(**a**)

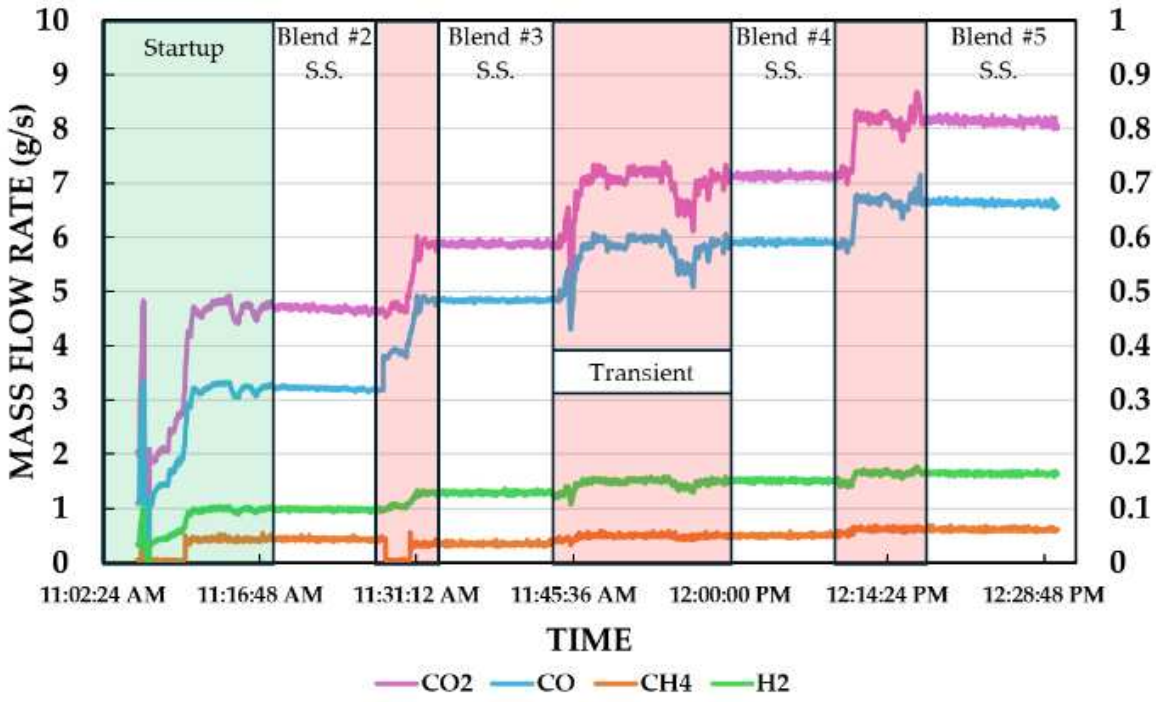

(**b**)

Figure 22. (a) Boost response during fuel blend transitions. **(b) Mass flow response** during fuel blend transitions.

The engine startup process, from cold start to achieving the expected load for Blend 1, consistently took about 15 minutes. Steady-state data for all blends were recorded at approximately 12-minute intervals. Because boost pressure was manually controlled, the supercharger speed was gradually increased to ensure proper operation of the zero-pressure regulator and avoid starving the engine of fuel. As shown in Figure 22a, many of the observed pressure peaks were due to input errors or overshoots relative to the required boost, which varied with environmental conditions. However, the transition times between Blend 3 to 4 showed an unusual behavior compared to the other blends, as shown in Figure 22b. From Blend 3 to 4 there is a peak in boost pressure, but the fuel mass flow decreases. According to the LabView code, the boost increase should have triggered a corresponding rise in fuel flow, as seen in the transition from Blend 4 to 5. This discrepancy could be due to a malfunction in the mass flow controllers, an error in the LabView code, or the boost pressure overpowering fuel flow. Despite this anomaly, the data suggests that, assuming the SOFC's expected mass flow is accurate and consistent, the engine could be controlled through the supercharger. Additionally, fuel composition changes in the real system should take about an hour for completion, giving the supercharger enough time to gradually increase its speed for a smoother transition.

By compiling all the experimental data, operational conditions were established to propose an engine control scheme. It was determined that simplifying engine controls is best achieved by maintaining ignition timing at 50° BTDC during all stages of operation. Additionally, to maximize BTE, the throttle should be set to 23% and the supercharger used to control boost pressure to achieve the pressures recorded in Figure 17. This adjustment not only enhances engine BTE but also reduces power consumption. It was found that the best way to control engine power is through the supercharger. Figure 23 shows a schematic of how the system would work. By measuring the

inlet manifold pressure and engine power output LabVIEW can adjust the supercharger speed and fuel flow based on the target power, i.e. SOFC load. With the throttle at a fixed position and ignition timing at 50° BTDC, max BTE can be achieved during all stages of operation.

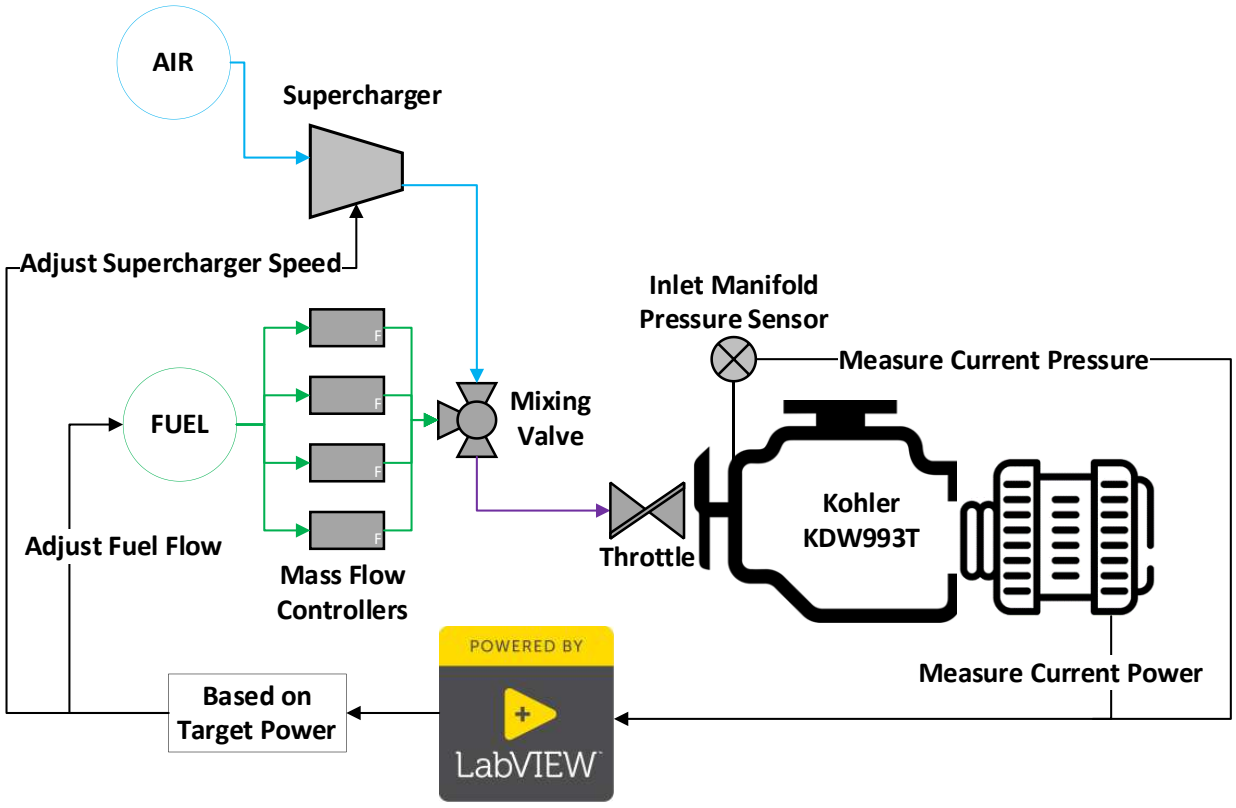

Figure 23. Automation schematic for maximum efficiency

CHAPTER 6. CONCLUSION

This research focused on operating an SI engine with fuel blends representative of the anode tail-gas from a pressurized SOFC and optimizing each composition for high efficiency operation and low power requirements. The results showed efficiencies as high as 31.4% at 1600 rpm, 17:1 CR, $\varphi = 0.75$, 50° BTDC, and 165 kPa of boost. The results also demonstrated the advantages of supplying the engine with the lowest boost to save on parasitic loads and increase BTE. Compared to the legacy data (Blend 1), the engine had a BTE decrease of 4.9%; however, the results were still satisfactory considering the reduction in LHV and load. In addition, it was found that a catalytic oxidizer is necessary to comply with emission regulations. The speed sweep confirmed that 1600 rpm is the optimal speed even with LHV reductions of up to 13% as compared with the legacy fuel blends and lower loads. With all the data gathered from these tests, operational conditions were generated to reliability maintain maximum efficiency at all stages of operation.

6.1 Future Work

Future work could include developing the control scheme for automation that would involve using the supercharger to regulate power with a constant throttle position. This would require the operational conditions to be coded into LabView and tested for experimental validation. Also, it would be beneficial to maintain a constant inlet manifold temperature for consistent performance. This could be achieved by having a more effective heat exchanger after the supercharger to cool the air. Further throttle calibration is required to mitigate the overlapping functionality of the trim valve and main throttle. The engine should be tested by operating with the developed control scheme on actual anode tail-gas from a SOFC rather than simulated gases.

REFERENCES

1. Donohoo-Vallett, P. *On The Path to 100% Clean Electricity Introduction to 100% Clean Electricity*; 2023;
2. United States Government What Is U.S. Electricity Generation by Energy Source? *https://www.eia.gov/tools/faqs/faq.php?id=427&t=3#:~:text=About%2060%25%20of%20this%20electricity,was%20from%20renewable%20energy%20sources.* **2024**.
3. United States Government How Many Power Plants Are in the United States?
4. United States Government Power Plant Data Highlights. **2023**.
5. Halinen, M.; Rautanen, M.; Saarinen, J.; Pennanen, J.; Pohjoranta, A.; Kiviaho, J.; Pastula, M.; Nuttall, B.; Rankin, C.; Borglum, B. Performance of a 10 KW SOFC Demonstration Unit. *ECS Trans* **2011**, *35*, 113–120, doi:10.1149/1.3569985.
6. Barelli, L.; Bidini, G.; Ottaviano, A. Integration of SOFC/GT Hybrid Systems in Micro-Grids. *Energy* **2017**, *118*, 716–728, doi:10.1016/j.energy.2016.10.100.
7. Colón Rodríguez, J.; Harun, N.F.; Zhou, N.; Sabolsky, E.; Tucker, D. *SYSTEM ANALYSIS OF A 100KW INTERNAL COMBUSTION ENGINE (ICE) SOLID OXIDE FUEL CELL (SOFC) HYBRID CONFIGURATION*; 2020;
8. Braun, R.; Floerchinger, G.; Wahlstrom, D.; Sullivan, N.P.; Vincent, T.; Danforth, R.; Bandhauer, T.; Olsen, D.; Windom, B. Development of a High-Efficiency, Low-Cost Hybrid SOFC/Internal Combustion Engine Power Generator. *ECS Trans* **2021**, *103*, 221–230, doi:10.1149/10301.0221ecst.
9. Michael Sprengel; Nick Echter Development and Optimization of a Solid Oxide Fuel Cell Gas Turbine Hybrid System.
10. O'Brien, C. Fuel Flexibility of SOFC Paves Path to Hydrogen Economy.
11. Kim, T.; Kang, S. Numerical Analysis of a Highly Efficient Cascade Solid Oxide Fuel Cell System with a Fuel Regenerator. *Appl Energy* **2023**, *341*, doi:10.1016/j.apenergy.2023.121114.
12. Zhou, J.; Wang, Z.; Han, M.; Sun, Z.; Sun, K. Optimization of a 30 KW SOFC Combined Heat and Power System with Different Cycles and Hydrocarbon Fuels. *Int J Hydrogen Energy* **2022**, *47*, 4109–4119, doi:10.1016/j.ijhydene.2021.11.049.

13. Langnickel, H.; Rautanen, M.; Gandiglio, M.; Santarelli, M.; Hakala, T.; Acri, M.; Kiviaho, J. Efficiency Analysis of 50 KWe SOFC Systems Fueled with Biogas from Waste Water. *Journal of Power Sources Advances* **2020**, *2*, doi:10.1016/j.powera.2020.100009.

14. Environmental Protection Agency, U.; Heat, C.; Partnership, P. *Catalog of CHP Technologies, Full Report*; 2017;

15. Mehran, M.T.; Khan, M.Z.; Song, R.H.; Lim, T.H.; Naqvi, M.; Raza, R.; Zhu, B.; Hanif, M.B. A Comprehensive Review on Durability Improvement of Solid Oxide Fuel Cells for Commercial Stationary Power Generation Systems. *Appl Energy* **2023**, *352*, doi:10.1016/j.apenergy.2023.121864.

16. Deangelis, D.; Karvountzi, G.; Minh, N.; Peter, M.; Rahman, F.; Sokolov, P.; Yang, D. *Solid Oxide Fuel Cell Hybrid System for Distributed Power Generation SOFC Scaleup for Hybrid and Fuel Cell Systems Final Topical Report Performed under DOE/NETL Cooperative Agreement*; 2004;

17. Nikiforakis, I.; Mamalis, S.; Assanis, D. Understanding Solid Oxide Fuel Cell Hybridization: A Critical Review. *Appl Energy* **2025**, *377*, 124277, doi:10.1016/j.apenergy.2024.124277.

18. Buonomano, A.; Calise, F.; d'Accadia, M.D.; Palombo, A.; Vicidomini, M. Hybrid Solid Oxide Fuel Cells-Gas Turbine Systems for Combined Heat and Power: A Review. *Appl Energy* 2015, *156*, 32–85.

19. Huang, S.; Yang, C.; Chen, H.; Zhou, N.; Tucker, D. Coupling Impacts of SOFC Operating Temperature and Fuel Utilization on System Net Efficiency in Natural Gas Hybrid SOFC/GT System. *Case Studies in Thermal Engineering* **2022**, *31*, doi:10.1016/j.csite.2022.101868.

20. Möller, B.F.; Arriagada, J.; Assadi, M.; Potts, I. Optimisation of an SOFC/GT System with CO2-Capture. *J Power Sources* **2004**, *131*, 320–326, doi:10.1016/j.jpowsour.2003.11.090.

21. Gengo, T.; Kobayashi, Y.; Ando, Y.; Hisatome, N. *Development of 200kW Class SOFC Combined Cycle System and Future View TATSUO KABATA* 2 KENICHIRO KOSAKA* 3*; 2008; Vol. 45;.

22. Burbank, W.; Witmer, D.D.; Holcomb, F. Model of a Novel Pressurized Solid Oxide Fuel Cell Gas Turbine Hybrid Engine. *J Power Sources* **2009**, *193*, 656–664, doi:10.1016/j.jpowsour.2009.04.004.

23. Kandepu, R.; Imsland, L.; Foss, B.A.; Stiller, C.; Thorud, B.; Bolland, O. Modeling and Control of a SOFC-GT-Based Autonomous Power System. *Energy* **2007**, *32*, 406–417.

24. Song, T.W.; Sohn, J.L.; Kim, T.S.; Ro, S.T. Performance Characteristics of a MW-Class SOFC/GT Hybrid System on a Commercially Available Gas Turbine. *Power Sources* **2006**, *158*, 361–367.

25. Calise, F.; Palombo, A.; Vanoli, L. Design and Partial Load Exergy Analysis of Hybrid–GT Power Plant. *Power Sources* **2006**, *158*, 225–244.

26. Yang, J.S.; Sohn, J.L.; Ro, S.T. Performance Characteristics of a Solid Oxide Fuel Cell/Gas Turbine System with Various Part-Load Control Modes. *Power Source* **2007**, *166*, 155–164.

27. Amba, G.; Rao, P.; Karthikeya Sharma, T. *Prospects of Hydrogen in HCCI Engines-A Review*; 2021; Vol. 16;.

28. Chehrmonavari, H.; Kakaee, A.; Hosseini, S.E.; Desideri, U.; Tsatsaronis, G.; Floerchinger, G.; Braun, R.; Paykani, A. Hybridizing Solid Oxide Fuel Cells with Internal Combustion Engines for Power and Propulsion Systems: A Review. *Renewable and Sustainable Energy Reviews* 2023, *171*.

29. Koo, T.; Kim, Y.S.; Lee, Y.D.; Yu, S.; Lee, D.K.; Ahn, K.Y. Exergetic Evaluation of Operation Results of 5-KW-Class SOFC-HCCI Engine Hybrid Power Generation System. *Appl Energy* **2021**, *295*, doi:10.1016/j.apenergy.2021.117037.

30. D.F. Chuahy, F.; Kokjohn, S.L. Solid Oxide Fuel Cell and Advanced Combustion Engine Combined Cycle: A Pathway to 70% Electrical Efficiency. *Appl Energy* **2019**, *235*, 391–408, doi:10.1016/j.apenergy.2018.10.132.

31. Zhu, P.; Yao, J.; Qian, C.; Yang, F.; Porpatham, E.; Zhang, Z.; Wu, Z. High-Efficiency Conversion of Natural Gas Fuel to Power by an Integrated System of SOFC, HCCI Engine, and Waste Heat Recovery: Thermodynamic and Thermo-Economic Analyses. *Fuel* **2020**, *275*, doi:10.1016/j.fuel.2020.117883.

32. Park, S.H.; Lee, Y.D.; Ahn, K.Y. Performance Analysis of an SOFC/HCCI Engine Hybrid System: System Simulation and Thermo-Economic Comparison. *Int J Hydrogen Energy* **2014**, *39*, 1799–1810, doi:10.1016/j.ijhydene.2013.10.171.

33. Choi, W.; Kim, J.; Kim, Y.; Song, H.H. Solid Oxide Fuel Cell Operation in a Solid Oxide Fuel Cell–Internal Combustion Engine Hybrid System and the Design Point Performance of the Hybrid System. *Appl Energy* **2019**, *254*, doi:10.1016/j.apenergy.2019.113681.

34. Choi, W.; Kim, J.; Kim, Y.; Kim, S.; Oh, S.; Song, H.H. Experimental Study of Homogeneous Charge Compression Ignition Engine Operation Fuelled by Emulated Solid Oxide Fuel Cell Anode Off-Gas. *Appl Energy* **2018**, *229*, 42–62, doi:10.1016/j.apenergy.2018.07.086.

35. Matthews, J.; Santoso, H.; Cheng, W.K. *Load Control for an HCCI Engine*; Michigan, 2005;

36. Song, H.H.; Edwards, C.F. Understanding Chemical Effects in Low-Load-Limit Extension of Homogeneous Charge Compression Ignition Engines via Recompression Reaction. *International Journal of Engine Research* **2009**, *10*, 231–250, doi:10.1243/14680874JER03409.

37. Nam, Y.; Kim, J.; Bahk, C.; Jang, I.; Song, H.H.; Lee, D. Modeling, Estimation, and Control of HCCI Engine with In-Cylinder Pressure Sensing. *Journal of Dynamic Systems, Measurement and Control, Transactions of the ASME* **2018**, *140*, doi:10.1115/1.4039210.

38. Kim, J.; Kim, Y.; Choi, W.; Ahn, K.Y.; Song, H.H. Analysis on the Operating Performance of 5-KW Class Solid Oxide Fuel Cell-Internal Combustion Engine Hybrid System Using Spark-Assisted Ignition. *Appl Energy* **2020**, *260*, doi:10.1016/j.apenergy.2019.114231.

39. Kim, J.; Kim, Y.; Song, H.H. Development of a New Configuration and Optimization of the 5-KW Class Energy Conversion System Combining a Solid Oxide Fuel Cell and Internal Combustion Engine Using a Spark-Assisted Ignition. *Energy Convers Manag* **2023**, *291*, doi:10.1016/j.enconman.2023.117329.

40. Ran, Z.; Longtin, J.; Assanis, D. Investigating Anode Off-Gas under Spark-Ignition Combustion for SOFC-ICE Hybrid Systems. *International Journal of Engine Research* **2022**, *23*, 830–845, doi:10.1177/14680874211016987.

41. Nikiforakis, I.; Ran, Z.; Sprengel, M.; Brackett, J.; Babbitt, G.; Assanis, D. Investigating Realistic Anode Off-Gas Combustion in SOFC/ICE Hybrid Systems: Mini Review and Experimental Evaluation. *International Journal of Engine Research* 2022, *23*, 876–892.

42. Padhi, G.; Windom, B.C.; Olsen, D.B.; Dandy, D. *THESIS MODELLING AND SIMULATION OF COMBUSTION OF DILUTE SYNGAS FUELS IN A CFR ENGINE Submitted By*; 2019;

43. Balu, A.; Olsen, D.; Windom, B.; Baker, D. *THESIS ANALYSIS OF SIMULATED DILUTE ANODE TAIL-GAS COMBUSTION CHARACTERISTICS ON A CFR ENGINE Submitted By*; 2020;

44. Countie, M.; Olsen, D.; Windom, B.; Baker, D. *THESIS PREDICTIVE MODELING AND TESTING OF A DIESEL DERIVED SOLID OXIDE FUEL CELL TAIL GAS SPARK-IGNITION ENGINE Submitted By*; 2020;

45. Castro, M.V.; Windom, B.C.; Marchese, A.J.; Daily, J. *THESIS COMPUTER-AIDED ENGINEERING AND DESIGN OF INTERNAL COMBUSTION ENGINES TO SUPPORT OPERATION ON NON-TRADITIONAL FUELS Submitted By*; 2020;

46. Broerman, E.; Blais, M.S.; Weyandt, N.; Renzi, P. Safety. In *Machinery and Energy Systems for the Hydrogen Economy*; Elsevier, 2022; pp. 521–542 ISBN 9780323903943.

47. Campari, A.; Ustolin, F.; Alvaro, A.; Paltrinieri, N. A Review on Hydrogen Embrittlement and Risk-Based Inspection of Hydrogen Technologies. *Int J Hydrogen Energy* 2023, *48*, 35316–35346.

48. Lee, J.A. *Hydrogen Embrittlement*; 2016;

49. Katsampes, N.; Montgomery, D.; Arney, G.; Olsen, D.B. Hydrogen-Natural Gas Fuel Blending in a "Rich Burn" Engine with 3-Way Catalyst. *Frontiers in Fuels* **2024**, *2*, doi:10.3389/ffuel.2024.1416716.

50. Cadigan, C.; Chmura, C.; Floerchinger, G.; Frankl, P.; Hunt, S.; Jensen, S.; Boushehri, C.; Vincent, T.L.; Braun, R.; Sullivan, N.P. Performance Characterization of Metal-Supported Solid-Oxide Fuel Cell Stacks at Elevated Pressure. *J Power Sources* **2023**, *573*, doi:10.1016/j.jpowsour.2023.233083.

51. Balu, A.; Bandhauer, T.; Windom, B.; Garland, S.; Braun, R.; Olsen, D.B. *Operation of a SI Engine Fueled by Simulated Exhaust Anode Tail-Gas from a SOFC*; 2019;

52. Balu, A.; Castro, M.; Padhi, G.; Bandhauer, T.; Windom, B.; Garland, S.; Olsen, D.; Braun, R. *OPTIMIZATION AND SIMULATION OF A CFR ENGINE FUELED BY DILUTE ANODE TAIL-GAS*; 2020;

53. Padhi, G.; Balu, A.; Garland, S.; Olsen, D.; Bandhauer, T.; Windom, B. *Combustion Modelling and Simulation of Dilute Syngas Fuels in a CFR Engine*; 2019;

54. Swartwout, Z.; Bandhauer, T.; Windom, B.; Garland, S.; Braun, R.; Olsen, D.B. *Optimizing Efficiency of an SI Engine Fueled by Simulated Anode Tail-Gas*; 2022;

55. Battista, R.A.; Hilt, M.B. *Low Heating Value Fuel Burning Capabilities of General Electric Industrial Gas Turbines*; 1982;

56. Krishnamoorthi, M.; Malayalamurthi, R.; He, Z.; Kandasamy, S. A Review on Low Temperature Combustion Engines: Performance, Combustion and Emission Characteristics. *Renewable and Sustainable Energy Reviews* 2019, *116*.

57. King, B.A.; Olsen, D.; Quinn, J.; Carter, E. *EXPERIMENTAL EVALUATION OF STACK TESTING METHODS FOR ACCURATE VOC MEASUREMENT*; 2019;

58. Urban, C.M.; Sharp, C.A. Computing Air/Fuel Ratio from Exhaust Composition. *ASME* **1994**, *24*.

59. SOUTHERN CALIFORNIA GAS COMPANY *Understanding SCAQMD Quality Rules for Engines*; 2009;

APPENDIX

APPENDIX A. ANALYZED ENGINE DATA AND RAW EMISSIONS

This section presents all the data used to generate the figures for the legacy data, alternator efficiency, and other results discussed. It also outlines the conditions under which each data point was recorded.

Table A1. Legacy ignition timing sweep analyzed data.

#	°BTDC	RPM	φ	T [N-m]	Mass flow [g/s]	BTE
1	15	1593.44	0.77	52.84	7.58	0.2981
2	20	1600.00	0.74	58.10	7.58	0.3289
3	25	1600.03	0.74	60.85	7.58	0.3446
4	30	1599.95	0.74	62.39	7.59	0.3532
5	35	1600.01	0.75	63.50	7.59	0.3595
6	**40**	**1600.02**	**0.74**	**63.65**	**7.59**	**0.3604**
7	45	1599.99	0.75	62.06	7.59	0.3512
8	50	1600.02	0.76	59.07	7.59	0.3344
9	55	1600.02	0.76	56.56	7.59	0.3203
10	60	1600.02	0.75	53.44	7.58	0.3027
11	65	1600.00	0.75	48.93	7.58	0.2771

Table A2. Legacy equivalence ratio sweep analyzed data.

#	°BTDC	RPM	φ	T [N-m]	Mass flow [g/s]	BTE
1	40	1600.03	0.66	61.41	7.58	0.3480
2	**40**	**1600.03**	**0.71**	**67.03**	**7.93**	**0.3630**
3	45	1600.01	0.75	73.07	8.65	0.3629
4	34	1600.01	0.80	63.75	7.58	0.3611
5	33	1600.01	0.85	63.07	7.58	0.3572
6	33	1600.00	0.90	61.96	7.59	0.3508
7	32	1600.06	0.94	61.14	7.59	0.3462
8	34	1599.98	1.01	58.98	7.58	0.3341
9	37	1599.96	1.06	53.36	7.58	0.3023

Table A3. Legacy data LHVs measured from the mass flow controllers.

		CO [g/s]	CO2 [g/s]	CH4 [g/s]	H2 [g/s]	Total [g/s]	SumController [g/s]	LHV [kJ/kg]
IGNITION SWEEP	15	0.6756	6.7004	0.0319	0.1760	7.5838	7.7122	3900.74
	20	0.6754	6.7010	0.0316	0.1762	7.5842	7.7089	3902.34
	25	0.6752	6.7003	0.0317	0.1761	7.5833	7.7467	3902.14
	30	0.6753	6.7019	0.0318	0.1762	7.5852	7.8121	3902.39
	35	0.6751	6.7052	0.0318	0.1762	7.5883	7.7623	3900.92
	40	0.6750	6.7049	0.0319	0.1761	7.5880	7.7970	3900.64
	45	0.6753	6.7024	0.0320	0.1761	7.5859	7.7373	3902.86
	50	0.6751	6.7037	0.0321	0.1760	7.5870	7.7380	3901.40
	55	0.6752	6.7024	0.0322	0.1759	7.5858	7.7230	3901.21
	60	0.6753	6.7016	0.0321	0.1759	7.5849	7.7214	3900.07
	65	0.6752	6.7002	0.0321	0.1759	7.5834	7.7629	3900.78

φ SWEEP	40, 0.65	0.6752	6.6981	0.0317	0.1759	7.5811	7.7234	3900.53
	40, 0.70	0.6754	6.6989	0.0319	0.1759	7.5820	7.8184	3900.61
	37, 0.75	0.6753	6.6982	0.0321	0.1758	7.5814	7.7943	3900.94
	34, 0.80	0.6750	6.7013	0.0322	0.1759	7.5844	7.7609	3900.86
	33, 0.85	0.6749	6.7015	0.0321	0.1759	7.5845	7.7760	3901.04
	33, 0.90	0.6751	6.7035	0.0319	0.1761	7.5866	7.7623	3901.47
	32, 0.95	0.6752	6.7022	0.0318	0.1761	7.5853	7.6206	3901.70
	34, 1.00	0.6750	6.7010	0.0316	0.1761	7.5838	7.8006	3900.96
	37, 1.05	0.6754	6.6995	0.0316	0.1760	7.5825	7.7402	3900.42
BOOST SWEEP	40, 1.48bar	0.6956	6.8647	0.0325	0.1807	7.7736	8.0030	3909.51
	40, 1.53bar	0.6955	6.8889	0.0327	0.1811	7.7982	7.9257	3904.09
	40, 1.59bar	0.6956	6.8902	0.0330	0.1810	7.7998	7.9272	3903.85
	40, 1.62bar	0.6951	6.8906	0.0330	0.1810	7.7997	8.0904	3903.69
	45, 1.58bar	0.7726	7.6397	0.0362	0.2006	8.6491	8.8402	3901.22
	45, 1.65bar	0.7727	7.6406	0.0365	0.2005	8.6503	8.7824	3900.90
	45, 1.66bar	0.7722	7.6415	0.0365	0.2006	8.6508	8.7563	3901.50
	45, 1.68bar	0.7725	7.6425	0.0366	0.2004	8.6519	8.7900	3899.72

Table A4. Alternator efficiency data.

208V Hot Power (We)	1600 RPM Eff (est)
1631.2	81.50%
2193.9	88.00%
5018.5	86.60%
7002.2	88.20%
9839.7	89.10%
11269	89.60%
12014.8	89.90%

Table A5. Ignition timing sweep analyzed data.

°BTDC	RPM	φ	kW	SumController [g/s]	BTE
BLEND #2 (SOFC LOAD = 50 %)					
60.00	1594.35	0.75	3.24	4.94	0.2326
55.00	**1603.62**	**0.75**	**3.29**	**4.94**	**0.2360**
50.00	1604.61	0.75	3.30	4.97	0.2354
45.00	1601.85	0.75	3.28	4.99	0.2329
40.00	1602.50	0.75	3.26	5.12	0.2258
35.00	1592.91	0.75	3.22	5.27	0.2166
30.00	1613.89	0.75	3.31	5.63	0.2087
BLEND #3 (SOFC LOAD = 75 %)					
60.00	1605.24	0.75	4.99	6.52	0.2604
55.00	1613.87	0.75	5.06	6.44	0.2673
50.00	**1601.58**	**0.75**	**5.01**	**6.30**	**0.2706**
45.00	1601.36	0.75	4.96	6.26	0.2695
40.00	1600.00	0.75	4.96	6.38	0.2645
35.00	1599.93	0.75	4.95	6.57	0.2568
30.00	1608.61	0.75	4.99	6.88	0.2471
BLEND #4 (SOFC LOAD = 100 %)					
60.00	1599.31	0.75	6.82	8.02	0.2875
55.00	1593.97	0.75	6.79	7.81	0.2940
50.00	**1596.14**	**0.75**	**6.81**	**7.77**	**0.2963**
45.00	1606.82	0.75	6.86	7.85	0.2953
40.00	1597.74	0.75	6.79	7.96	0.2882
35.00	1598.62	0.75	6.79	8.27	0.2776
30.00	1605.68	0.75	6.84	8.68	0.2661

BLEND #5 (SOFC LOAD = 125 %)					
60.00	1603.30	0.75	8.02	9.10	0.3043
55.00	1600.16	0.75	8.04	8.98	0.3088
50.00	**1610.50**	**0.75**	**8.17**	**9.10**	**0.3099**
45.00	1600.49	0.75	7.98	9.05	0.3042
40.00	1598.78	0.75	7.95	9.28	0.2957
35.00	1596.51	0.75	7.91	9.61	0.2842
30.00	1606.30	0.75	8.01	10.27	0.2733

Table A6. New blends LHVs measured from the mass flow controllers for the ignition timing sweep.

		CO [g/s]	CO2 [g/s]	CH4 [g/s]	H2 [g/s]	Total [g/s]	SumController [g/s]	LHV [kJ/kg]
BLEND #2	30	0.3508	5.1197	0.0473	0.1072	5.6250	5.6254	3340.76
	35	0.3287	4.7966	0.0444	0.1004	5.2700	5.2700	3341.55
	40	0.3191	4.6565	0.0432	0.0975	5.1163	5.1164	3342.85
	45	0.3115	4.5442	0.0421	0.0951	4.9929	4.9929	3341.79
	50	0.3101	4.5211	0.0418	0.0947	4.9677	4.9677	3343.30
	55	0.3081	4.4937	0.0418	0.0942	4.9377	4.9378	3345.48
	60	0.3080	4.4919	0.0415	0.0941	4.9355	4.9353	3343.23
BLEND #3	30	0.5101	6.1973	0.0363	0.1359	6.8797	6.8804	3389.26
	35	0.4873	5.9146	0.0346	0.1298	6.5664	6.5661	3390.50
	40	0.4732	5.7448	0.0341	0.1261	6.3782	6.3786	3394.98
	45	0.4649	5.6407	0.0331	0.1239	6.2627	6.2626	3393.63
	50	0.4675	5.6743	0.0335	0.1246	6.2999	6.3001	3393.41
	55	0.4781	5.8011	0.0340	0.1275	6.4407	6.4409	3394.15
	60	0.4839	5.8734	0.0346	0.1290	6.5208	6.5207	3393.34

BLEND #4	30	0.6470	7.8154	0.0549	0.1656	8.6829	8.6834	3362.78
	35	0.6159	7.4425	0.0522	0.1576	8.2682	8.2683	3360.30
	40	0.5933	7.1654	0.0503	0.1518	7.9608	7.9609	3362.02
	45	0.5853	7.0693	0.0495	0.1497	7.8539	7.8540	3360.43
	50	0.5787	6.9918	0.0491	0.1480	7.7676	7.7674	3360.82
	55	0.5818	7.0266	0.0493	0.1488	7.8065	7.8066	3360.52
	60	0.5975	7.2175	0.0505	0.1529	8.0184	8.0185	3360.44
BLEND #5	30	0.6892	9.3212	0.0697	0.1883	10.2684	10.2681	3221.95
	35	0.7067	8.6641	0.0647	0.1750	9.6105	9.6102	3269.52
	40	0.6823	8.3683	0.0625	0.1691	9.2822	9.2822	3269.96
	45	0.6658	8.1623	0.0610	0.1649	9.0540	9.0536	3270.39
	50	0.6688	8.1998	0.0612	0.1658	9.0957	9.0959	3272.03
	55	0.6604	8.0953	0.0604	0.1638	8.9798	8.9799	3272.50
	60	0.6691	8.2019	0.0611	0.1657	9.0979	9.0979	3269.55

Table A7. Supercharger boost sweep analyzed data.

BLEND #2 (SOFC LOAD = 50%)		**TIMING: 55°**	
	Ignition Timing Data	Lower Limit	Upper Limit
RPM	**1603.32**	1598.26	1599.96
φ	**0.75**	0.75	0.75
kW	**3.29**	3.25	3.27
SumController [g/s]	**4.94**	4.97	5.01
BTE	**23.60**	23.21	23.15
Booster Air [kPa]	**100.31**	94.96	122.00
Inlet Manifold Pressure [kPa]	**89.85**	95.34	96.46
Throttle Position [%]	**17.27**	22.14	6.76
Boost Consumed Power [W]	**N/A**	228.00	388.80

BLEND #3 (SOFC LOAD = 75%)		**TIMING: 50°**	
	Ignition Timing Data	Lower Limit	Upper Limit
RPM	1601.58	**1606.84**	1600.19
φ	0.75	**0.75**	0.75
kW	5.01	**5.13**	5.07
SumController [g/s]	6.30	**6.42**	6.39
BTE	27.06	**27.22**	27.05
Booster Air	118.00	**123.58**	179.10
Inlet Manifold [kPa] Pressure [kPa]	112.18	**119.37**	118.89
Throttle Position [%]	21.56	**16.26**	4.17
Boost Consumed Power [W]	N/A	**528.00**	1075.20

BLEND #4 (SOFC LOAD = 100%)		**TIMING: 50°**	
	Ignition Timing Data	Lower Limit	Upper Limit
RPM	1596.14	**1600.14**	1600.00
φ	0.75	**0.75**	0..75
kW	6.81	**6.90**	6.85
SumController [g/s]	7.77	**7.82**	8.06
BTE	29.63	**29.89**	29.67
Booster Air	147.21	**145.21**	204.11
Inlet Manifold [kPa] Pressure [kPa]	139.99	**143.13**	145.43
Throttle Position [%]	17.33	**22.10**	5.00
Boost Consumed Power [W]	N/A	**907.20**	1588.80

BLEND #5 (SOFC LOAD = 125%)		TIMING: 50°	
	Ignition Timing Data	Lower Limit	Upper Limit
RPM	1610.50	**1592.74**	1600.96
φ	0.75	**0.75**	0.75
kW	8.17	**8.22**	8.26
SumController [g/s]	9.10	**9.05**	9.31
BTE	30.99	**31.41**	31.41
Booster Air	180.67	**165.33**	182.64
Inlet Manifold [kPa] Pressure [kPa]	161.88	**164.22**	167.36
Throttle Position [%]	13.36	**22.29**	12.25
Boost Consumed Power [W]	N/A	**1296.00**	1617.60

Table A8. Ignition timing sweep with parasitic losses at the lower limit

BLEND #2 (SOFC LOAD = 50 %)					
°BTDC	RPM	φ	kW	SumController [g/s]	BTE
60.00	1594.35	0.75	3.01	4.94	0.2163
55.00	**1603.62**	**0.75**	**3.06**	**4.94**	**0.2196**
50.00	1604.61	0.75	3.07	4.97	0.2191
45.00	1601.85	0.75	3.05	4.99	0.2167
40.00	1602.50	0.75	3.03	5.12	0.2100
35.00	1592.91	0.75	2.99	5.27	0.2013
30.00	1613.89	0.75	3.08	5.63	0.1943
BLEND #3 (SOFC LOAD = 75 %)					
60.00	1605.24	0.75	4.47	6.52	0.2331
55.00	1613.87	0.75	4.54	6.44	0.2396
50.00	**1601.58**	**0.75**	**4.49**	**6.30**	**0.2423**
45.00	1601.36	0.75	4.44	6.26	0.2411
40.00	1600.00	0.75	4.44	6.38	0.2366

35.00	1599.93	0.75	4.43	6.57	0.2296
30.00	1608.61	0.75	4.47	6.88	0.2212
BLEND #4 (SOFC LOAD = 100 %)					
60.00	1599.31	0.75	5.91	8.02	0.2493
55.00	1593.97	0.75	5.88	7.81	0.2547
50.00	**1596.14**	**0.75**	**5.90**	**7.77**	**0.2569**
45.00	1606.82	0.75	5.95	7.85	0.2562
40.00	1597.74	0.75	5.88	7.96	0.2497
35.00	1598.62	0.75	5.88	8.27	0.2405
30.00	1605.68	0.75	5.93	8.68	0.2308
BLEND #5 (SOFC LOAD = 125 %)					
60.00	1603.30	0.75	6.72	9.10	0.2552
55.00	1600.16	0.75	6.74	8.98	0.2591
50.00	**1610.50**	**0.75**	**6.87**	**9.10**	**0.2607**
45.00	1600.49	0.75	6.68	9.05	0.2548
40.00	1598.78	0.75	6.65	9.28	0.2475
35.00	1596.51	0.75	6.61	9.61	0.2376
30.00	1606.30	0.75	6.71	10.27	0.2291

Table A9. Speed sweep analyzed data.

BLEND #4 (SOFC LOAD = 100 %)					
°BTDC	RPM	φ	kW	SumController [g/s]	BTE
60.00	1797.92	0.75	6.66	10.27	0.2199
50.00	**1600.14**	**0.75**	**6.90**	**7.82**	**0.2989**
45.00	1392.69	0.75	5.93	11.14	0.1767

Table A10. New blends LHVs measured from the mass flow controllers for the boost timing sweep.

	CO [g/s]	CO2 [g/s]	CH4 [g/s]	H2 [g/s]	Total [g/s]	SumController [g/s]	LHV [kJ/kg]
BLEND #2							
Upper	0.3127	4.5604	0.0419	0.0955	5.0106	5.0105	3340.32
Lower	0.3101	4.5199	0.0415	0.0947	4.9661	4.9660	3341.36
BLEND #3							
Upper	0.4739	5.7528	0.0336	0.1262	6.3866	6.3863	3389.38
Lower	0.4763	5.7786	0.0338	0.1269	6.4156	6.4159	3391.91
BLEND #4							
Upper	0.4864	7.3658	0.0514	0.1559	8.0595	8.0594	3254.11
Lower	0.5826	7.0360	0.0489	0.1488	7.8162	7.8161	3355.49
BLEND #5							
Upper	0.5865	8.4850	0.0631	0.1714	9.3060	9.3062	3190.10
Lower	0.6605	8.1655	0.0606	0.1650	9.0515	9.0515	3263.79

APPENDIX B. EMISSION ANALYSIS

The following section presents all the data used to generate the figures for the emission results. It also includes the estimation process used for the emission samples.

Table B1. BTE for each fuel composition during emission testing.

	RPM	φ	kW	SumController [g/s]	BTE
BLEND #2	1610.10	0.75	3.28	5.18	**22.47**
BLEND #3	1602.40	0.75	5.04	6.52	**26.33**
BLEND #4	1598.59	0.75	6.68	7.93	**28.50**
BLEND #5	1589.02	0.75	8.22	9.23	**30.74**

Table B2. Raw Five-gas emissions.

	CO2 [%]	O2 [%]	THC [ppm]	CO [ppm]	NOx [ppm]
BLEND #2	28.3267	7.059551	466.4659	2860.731	3.52604
BLEND #3	28.89676	6.864678	232.773	2582.732	4.492637
BLEND #4	28.89054	6.810778	318.6553	2655.636	5.291266
BLEND #5	29.06182	6.872473	392.9327	2954.484	4.845675

Table B3. Raw FTIR emissions.

	CO2 [%]	H2O [%]	THC_{wet} [ppm]	CO [ppm]	NOx [ppm]
BLEND #2	17.63	0.26	5.13	26.89	5.23
BLEND #3	7.03	0.23	5.10	27.09	0.90
BLEND #4	8.01	0.24	5.08	27.19	0.98
BLEND #5	9.94	0.27	5.06	27.61	1.42

Table B4. Solved perfect lean combustion reaction for each blend.

Const.	# Moles	X_i	PPM_i	%$_i$	MW_i	
			Blend #2			
CO2	0.7136	0.1024	102385.8	10.24	44.01	g/mol
H2O	0.3186	0.0457	45713.1	4.571	18.02	g/mol
O2	1.0822	0.1553	155277.5	15.53	32.00	g/mol
N2	4.8550	0.6966	696623.6	69.66	28.02	g/mol
	6.97	1.00			29.82	g/mol
			Blend #3			
CO2	0.7058	0.1025	102491.9	10.25	44.01	g/mol
H2O	0.3143	0.0456	45632.9	4.563	18.02	g/mol
O2	1.0691	0.1552	155241.7	15.52	32.00	g/mol
N2	4.7975	0.6966	696633.5	69.66	28.02	g/mol
	6.89	1.00			29.82	g/mol
			Blend #4			
CO2	0.7136	0.1030	102952.3	10.30	44.01	g/mol
H2O	0.3106	0.0448	44806.0	4.481	18.02	g/mol
O2	1.0770	0.1554	155389.8	15.54	32.00	g/mol
N2	4.8299	0.6969	696851.9	69.69	28.02	g/mol
	6.93	1.00			29.84	g/mol
			Blend #5			
CO2	0.7229	0.1031	103089.8	10.31	44.01	g/mol
H2O	0.3032	0.0432	43240.5	4.324	18.02	g/mol
O2	1.0958	0.1563	156269.9	15.63	32.00	g/mol
N2	4.8903	0.6974	697399.8	69.74	28.02	g/mol
	7.01	1.00			29.86	g/mol

APPENDIX C. ENGINE SKID, ECU, AND BALANCE OF PLANT

This section shows sensors for the engine skid testing, stock engine specifications, ECU spec sheet and software, and the instrumentation balance of plant. These piping and instrumentation diagrams (P&IDs) include the majority of the systems used for testing. However, these figures do not represent the complete system nor are they the final versions; rather, they are P&IDs representative of the overall components.

Table C1. Stock engine specification

Displacement	0.993L
Configuration	Inline 3 Cylinder
Compression Ratio	21:1
Injection	Unit pump injector with swirl pre-chamber
Forced Induction	Turbocharger with internal wastegate
Power	41.9 kW at 4500 RPM
Torque	96.5 N*m at 3800 RPM
Minimum BSFC	238.6 g/kWh at 2600 RPM
Maximum Speed	4600 RPM

Table C2. Engine sensors.

Kohler KDW1002 Sensors	
Pressure transducer	626-09-GH-P1-E1-S1
Thermocouple	KQXL-116G-12
Cam sensor	MSD2348
Crank sensor	25375909
Lambda sensor	LSU 4.9

Table C3. SECM70 standard features

Woodward SECM70
• 2 engine speed inputs: camshaft and crankshaft speed (crank software configurable for variable reluctance [VR] magnetic pickup sensor or Hall effect proximity sensor inputs) • 1 frequency input • Up to 16 analog inputs • 4 switch inputs • Up 2 HEGO sensor inputs • 1 UEGO sensor input (compatible with Bosch LSU4.9 or NTK sensors) • Up to 2 knock sensor inputs • 1 transducer power output providing +5 V (350 mA) • Up to 6 injector drivers (3 capable of providing software configurable peak-and-hold current levels • Up to 8 ignition coil drivers • MPRD (Master Power Relay Driver) low-side output • 9 low-side output drivers (up to 3 with current sense feedback) • Up to 3 lamp drivers • TACH low-side output • 2 H-bridge driver outputs providing 10 A and 5 A drive capability and current-sense feedback • Optional 3-Phase BLDC driver • 2 CAN (Controller Area Network) communications ports • 16-kilobyte serial EEPROM for tunable parameter storage

Figure C1. PG+ Main Page

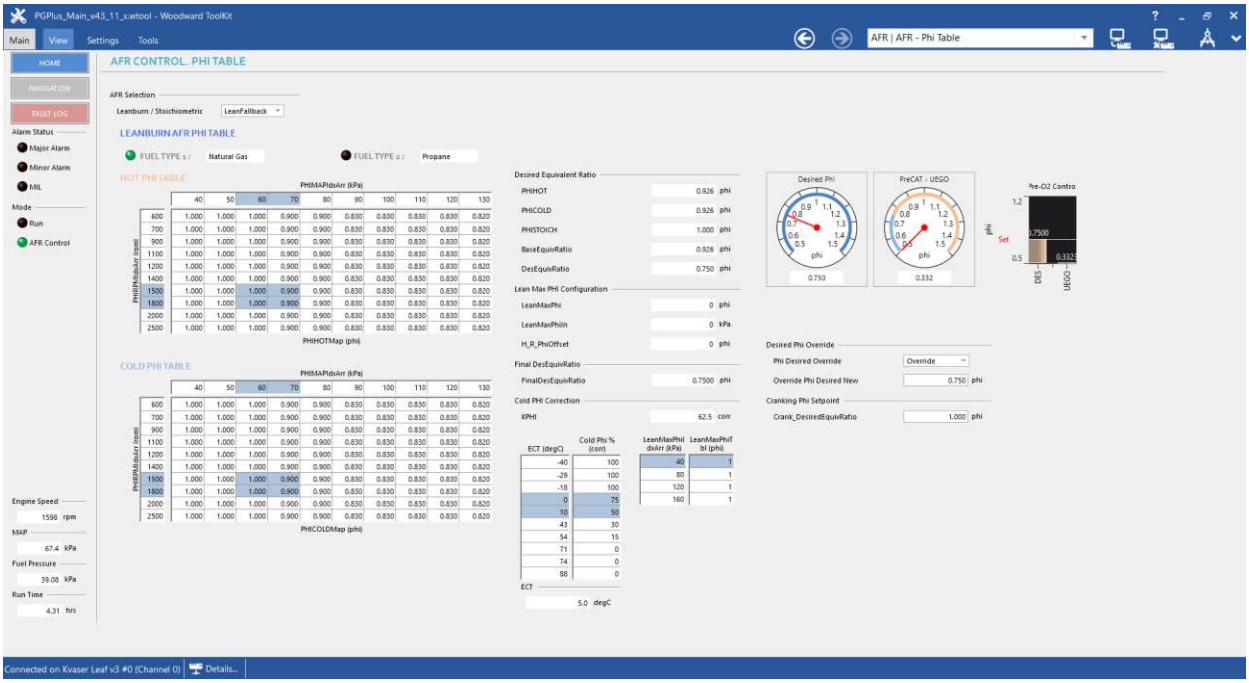

Figure C2. PG+ Equivalence ratio setpoint

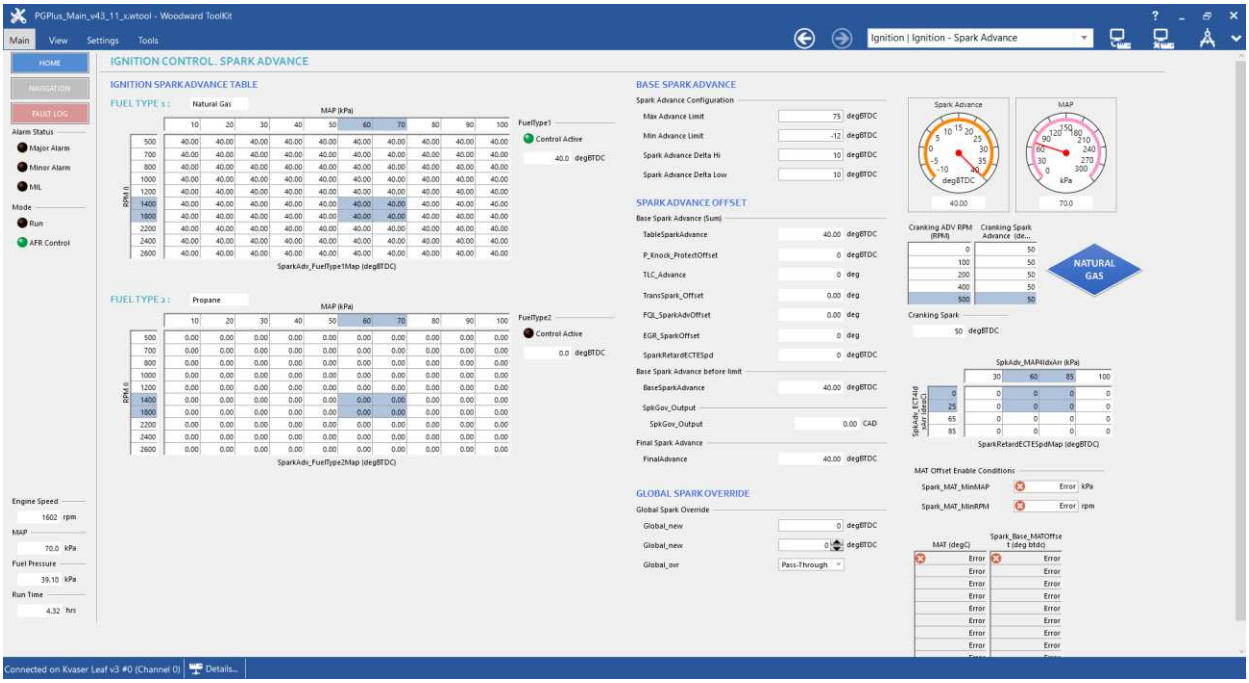

Figure C3. PG+ Ignition timing setpoint

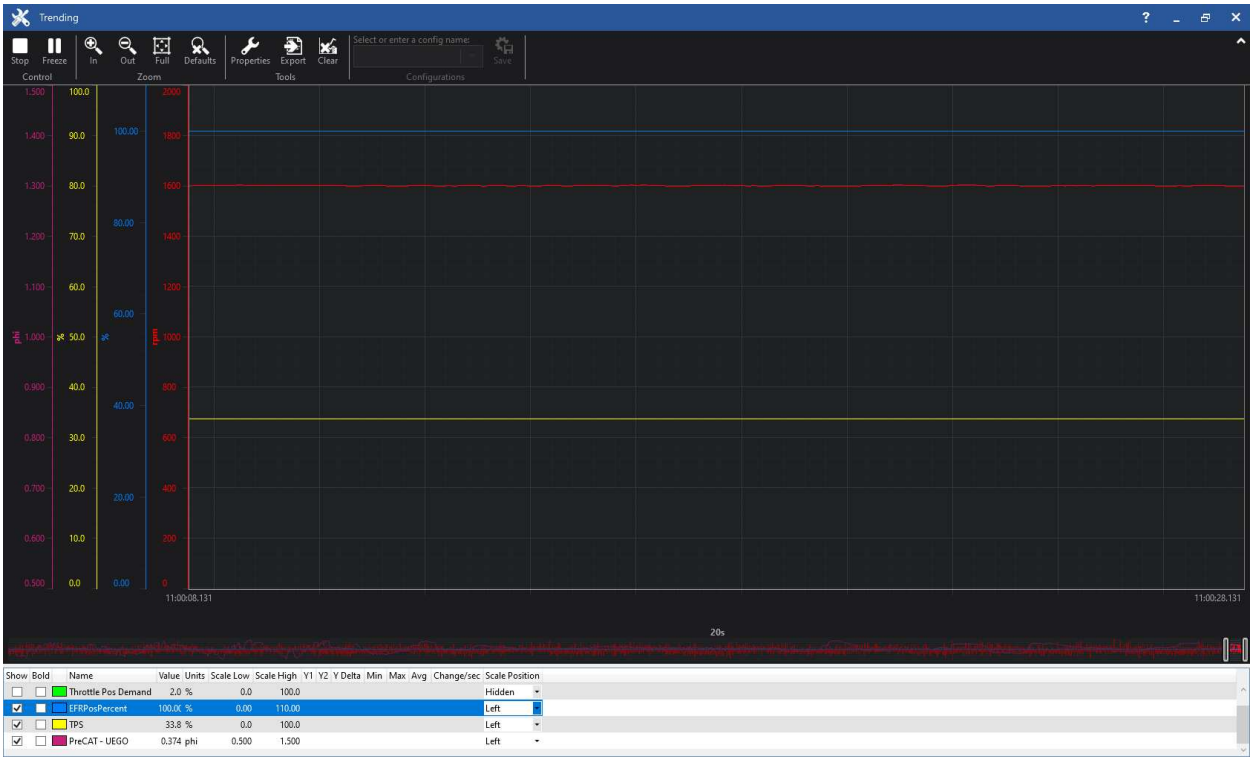

Figure C4. PG+ Trendline Monitoring

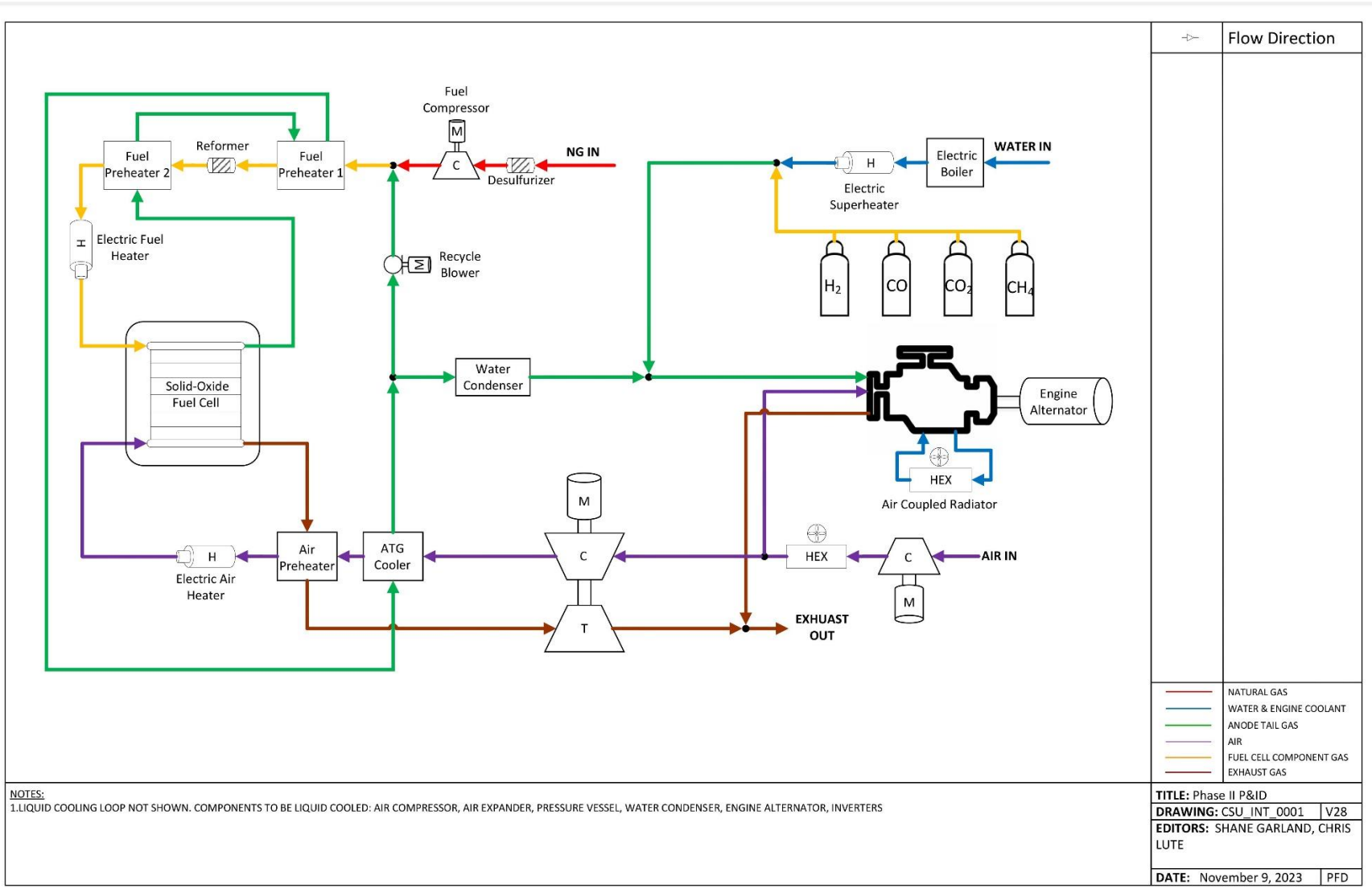

Figure C5. Overall facility operation.

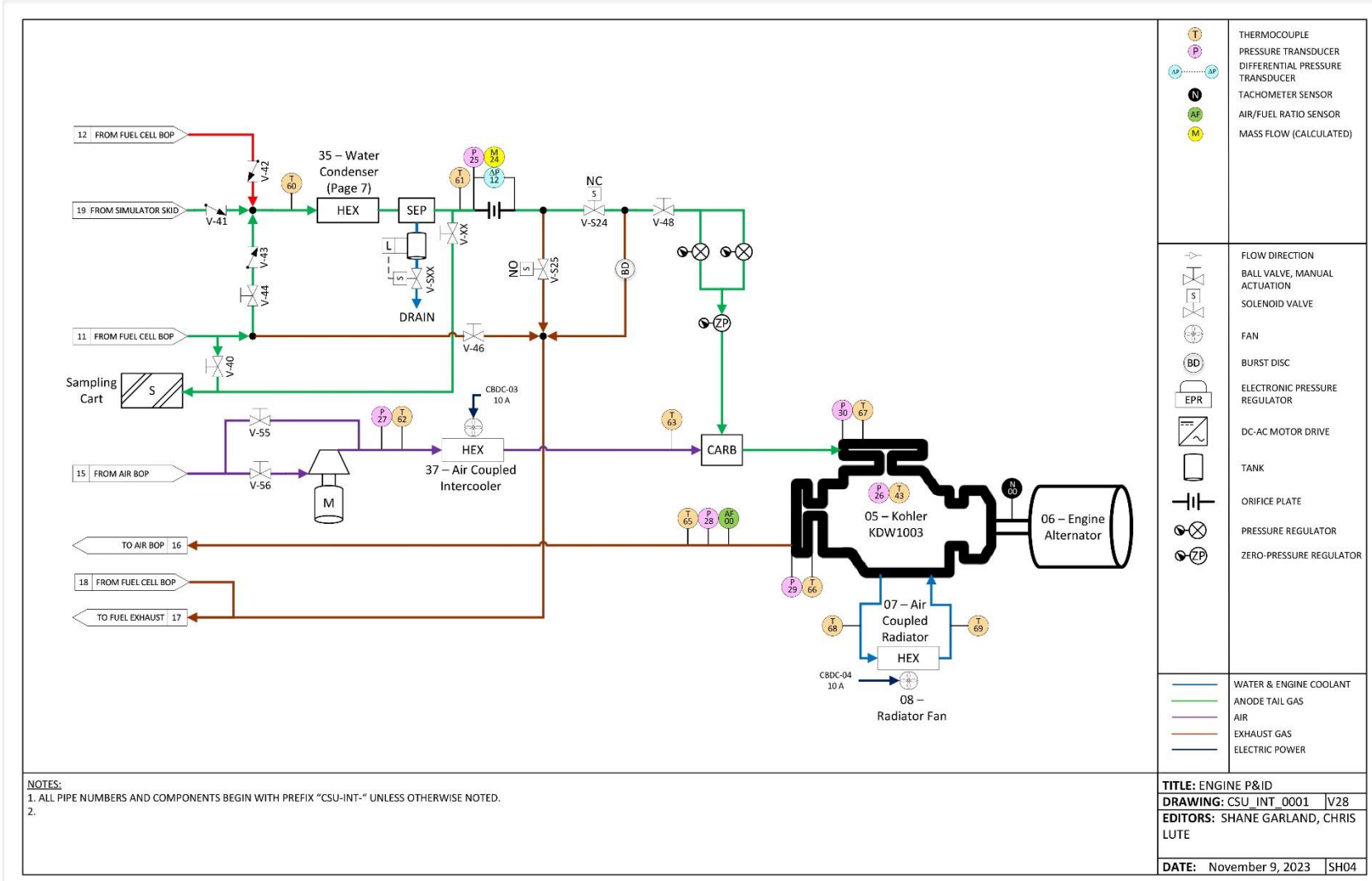

Figure C6. Detail engine skid components.

ABBREVIATIONS

Symbol	Description	Unit
SOFC	*solid oxide fuel cell*	-
GT	*gas turbine*	-
ICE	*internal combustion engine*	-
HCCI	*homogeneous charge compression ignition*	-
CI	*compression ignition*	-
SI	*spark ignition*	-
CFR	*cooperative fuel research*	-
BTDC	*before top dead center*	° BTDC
CAD	*crank degree angle*	° CAD
ECU	*engine control unit*	-
Φ	*equivalence ratio*	-
NG	*natural gas*	-
Hg	*mercury*	-
SO2	*sulfur dioxide*	-
NH4	*ammonia*	-
CO	*carbon monoxide*	-
CH4	*methane*	-
H2	*hydrogen*	-

N2	*nitrogen*	-
FTIR	*Fourier transform infrared spectroscopy*	-
CO2	*carbon dioxide*	-
H2O	*water*	-
NOx	*nitrous oxide*	-
C	*Celsius*	° C
$/kW	*dollars per kilowatt*	-
BSTHC	*brake specific total hydrocarbons*	g/bkW-hr
BSCO	*brake specific carbon monoxide*	g/bkW-hr
BSNOx	*brake specific nitrous oxide*	g/bkW-hr
U.S.	*United Stated of America*	-
EPA	*Environmental Protection Agency*	-
CSU	*Colorado State University*	-
EES	*Engineering Equation Solver*	-
P&ID	*piping and instrumentation diagrams*	-
THC	*total hydrocarbons*	ppm